Asymmetric thermal evolution of the Moon

M. Laneuville, M. Wieczorek, D. Breuer, N. Tosi

JOURNAL OF GEOPHYSICAL RESEARCH: PLANETS, VOL. 118, 1435–1452, doi:10.1002/jgre.20103, 2013

Asymmetric thermal evolution of the Moon

M. Laneuville,[1] M. A. Wieczorek,[1] D. Breuer,[2] and N. Tosi[3]

Received 11 February 2013; revised 17 June 2013; accepted 18 June 2013; published 17 July 2013.

[1] The Moon possesses a clear dichotomy in geological processes between the nearside and farside hemispheres. The most pronounced expressions of this dichotomy are the strong concentration of radioactive heat sources on the nearside in a region known as the Procellarum KREEP Terrane (PKT) and the mare basaltic lava flows that erupted in or adjacent to this terrane. We model the thermochemical evolution of the Moon using a 3-D spherical thermochemical convection code in order to assess the consequences of a layer enriched in heat sources below the PKT on the Moon's global evolution. We find that in addition to localizing most of the melt production on the nearside, such an enriched concentration of heat sources in the PKT crust has an influence down to the core-mantle boundary and leaves a present-day temperature anomaly within the nearside mantle. Moderate gravitational and topographic anomalies that are predicted in the PKT, but not observed, may be masked either by crustal thinning or gravitational anomalies from dense material in the underlying mantle. Our models also predict crystallization of an inner core for sulfur concentrations less than 6 wt %.

Citation: Laneuville, M., M. A. Wieczorek, D. Breuer, and N. Tosi (2013), Asymmetric thermal evolution of the Moon, *J. Geophys. Res. Planets*, *118*, 1435–1452, doi:10.1002/jgre.20103.

1. Introduction

[2] The asymmetric distribution of lunar volcanism became apparent when the farside of the Moon was imaged for the first time by the Soviet mission Luna 3 in 1959. It was surprising to realize that almost no basaltic lava flows were present on the farside and that most of the lunar maria were located on the nearside. Whereas about one third of the nearside hemisphere of the Moon has been resurfaced by basaltic lava flows, only about 1% of the farside is covered, principally within a few large impact basins such as South Pole, Aitken, Moscoviense, and Apollo. Dating of the lunar samples, in combination with crater counting techniques, showed that mare basalts on the nearside range in age from about 4 to 1 Ga [*Hiesinger et al.*, 2003] and those on the farside from 3 to 2.5 Ga [*Haruyama et al.*, 2009]. Taking into account the likelihood that older volcanism is now buried either below the maria or beneath the ejecta blankets of large ancient impact basins, the total duration of volcanism is greater than 3 billion years [*Antonenko et al.*, 1995].

[3] Analyses of Apollo γ-ray measurements and the thorium content of lunar samples suggested that heat-producing elements were localized on the nearside of the Moon [*Metzger et al.*, 1977; *Warren and Wasson*, 1980; *Haskin*, 1998], but it was not until the *Lunar Prospector* mission in 1998 that the global distribution of heat-producing elements was mapped [*Lawrence et al.*, 1998]. As shown in Figure 1, a high concentration of incompatible elements, in particular thorium and uranium, was observed on the nearside in a region strongly correlated with the maria [*Lawrence et al.*, 1998], suggesting a genetic link between the two. Since thorium and uranium are usually the main heat sources that affect a planet's thermal evolution, their asymmetric distribution most likely leads to an asymmetric magmatic and geologic evolution [*Wieczorek and Phillips*, 2000].

[4] *Jolliff et al.* [2000] defined the region of high thorium concentration on the nearside as the Procellarum KREEP Terrane (PKT), where the acronym KREEP stands for potassium, rare earth elements, and phosphorus, which occupies about 17% of the lunar surface, or one third of the nearside hemisphere. Nonmare materials excavated from beneath mare basalts show high thorium concentrations as well, implying that KREEP is not solely enriched in the near-surface lava flows, but also in the underlying crust [*Jolliff et al.*, 2000]. Furthermore, the PKT contains both highlands and volcanic flows, both of which can have high thorium concentrations. The total extent of the concentration of heat sources in the crust is somewhat uncertain, as it is not simple to determine the composition of the deep crust. Nevertheless, the lack of KREEP signatures in the material ejected from large impact basins, such as Crisium, Humboldtianum, Moscoviense, and Orientale, implies that KREEP in the crust is localized to the nearside hemisphere [see, e.g., *Warren*,

[1]Department of Planetary and Space Sciences, Institut de Physique du Globe de Paris, Paris, France.
[2]Department of Planetary Physics, German Aerospace Center, Berlin, Germany.
[3]Department of Planetary Geodesy, Technische Universität Berlin, Berlin, Germany.

Corresponding author: M. Laneuville, Department of Planetary and Space Sciences, Institut de Physique du Globe de Paris, Case 7071, Lamarck A 35, rue Hélène Brion Université Paris Diderot 75205, Paris Cedex 13, France. (laneuville@ipgp.fr)

2169-9097/13/10.1002/jgre.20103

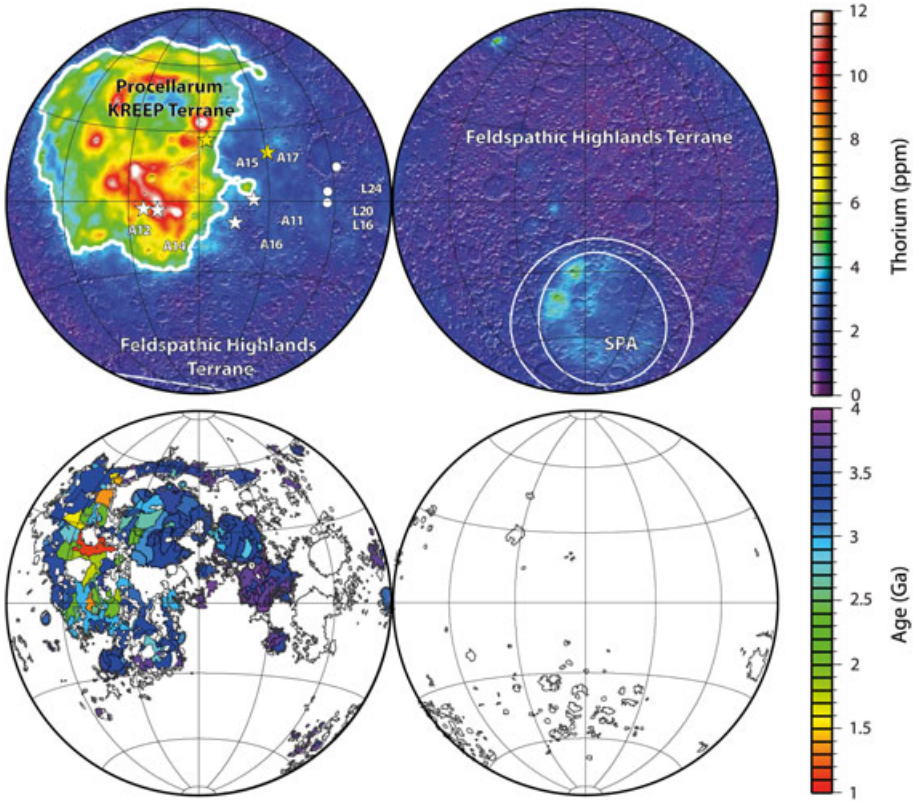

Figure 1. (top) *Lunar Prospector* surface thorium concentrations of *Lawrence et al.* [2003]. The PKT is outlined in white and is defined by the 4 ppm thorium contour. Stars are the Apollo landing sites, and the circles are the Luna sample return sites. The yellow stars are the locations of the two Apollo heat flow measurements. The farside ellipses are the inner compositional anomaly and outer structural rim of the South Pole-Aitken basin. The nearside is on the left, the farside on the right and the projection is Lambert azimuthal equal area (image modified from *Mimoun et al.* [2012]). (bottom) Mare basalt ages map of the nearside using data from *Hiesinger et al.* [2003] and the mare basalt map from the U.S. Geological Survey. These maps suggest that volcanism and crustal heat sources are genetically related.

2001]. Furthermore, a recent study on the viscoelastic deformation of lunar impact basins also suggests that the farside crust is depleted in radioactive elements with respect to the crust within the PKT [*Kamata et al.*, 2013].

[5] It is widely accepted that the Moon formed hot and that part of its outer layers was molten to form what is known as the lunar magma ocean. As the magma ocean crystallized, the remaining liquid became progressively enriched in incompatible elements. When plagioclase began to crystallize, it was lighter than the surrounding liquid and rose to form the crust. The last part of the magma ocean to crystallize formed a highly evolved layer between the crust and mantle composed of materials enriched in KREEP and also in iron-rich minerals such as ilmenite. The KREEP layer was once thought to form a global layer that was about 2 km thick [*Warren and Wasson*, 1979], but some process appears to have concentrated this material within the present-day PKT, forming an equivalent layer that might be about 10 km thick.

[6] Three different classes of models have been proposed to explain this wide-scale segregation. *Wasson and Warren* [1980] first suggested that the crystallization of the magma ocean was asymmetric. A locally thicker crust on the farside would give rise to a thinner underlying magma ocean, and thus concentrate KREEP-rich materials on the nearside, where the crust is thinnest. This model requires an initially thicker crust on the farside, possibly caused by a giant impact on the nearside [*Neumann et al.*, 1996; *Byrne*, 2007], or a global convection pattern within the magma ocean that could have transported crust preferentially to the farside [*Loper and Werner*, 2002].

[7] Second, *Zhong et al.* [2000] assumed that a global layer of dense, late-stage ilmenite cumulates quickly sank to the core-mantle boundary, carrying along with it a large fraction of the KREEP layer. This layer then became hot and unstable and rose again on the nearside as a degree-1 upwelling, explaining both the present-day distribution of heat sources and the timing of volcanism. A more recent study by *Qin et al.* [2012] showed that the correlation between deep moonquakes and mare basalt could be the consequence of this ilmenite cumulate layer, if it was enriched in water. A related model, proposed by *Parmentier et al.* [2002], showed that the downwelling of a mixed ilmenite cumulate layer itself could follow a degree-1 pattern and concentrate KREEP beneath the PKT (though, see also *Elkins-Tanton et al.* [2002] for comments about that model).

[8] Finally, impacts are often invoked to explain KREEP localization. *Ghods and Arkani-Hamed* [2007] showed that impacts would generate subsurface thermal anomalies that might redistribute KREEP-rich materials located beneath the crust. Depending on their size, the impacts would either mix

this layer into the underlying mantle or simply concentrate KREEP at the edge of the basin, thus enhancing volcanic activity there. Another view involving impact is from *Jutzi and Asphaug* [2011] who claimed that a low-velocity impact from a 1200 km diameter companion to our moon might have displaced the global KREEP-rich layer to the nearside.

[9] Regardless of the origin of the PKT, its bare existence is expected to have completely changed the subsequent post-magma ocean thermal evolution of the Moon. The influence of the PKT on lunar evolution has already been investigated by *Wieczorek and Phillips* [2000] and *Hess and Parmentier* [2001], but these studies used highly simplified thermal models. *Wieczorek and Phillips* [2000] developed an axially symmetric 3-D conduction model which showed that partial melting of the underlying mantle is an inevitable outcome of a thick KREEP layer on the nearside hemisphere and that volcanism should span most of lunar history. This result was confirmed by *Hess and Parmentier* [2001] in a 1-D thermal conduction study but they also noted that the wide, partially molten region caused by that layer could form an impenetrable barrier to the eruption of mare basalts. They concluded that the hypothesis of a thickened KREEP layer below the PKT imposed strong constraints on the concentration of heat sources in the PKT and crustal thickness to remain consistent with both geological and petrological observations. Recently, *Grimm* [2013] re-analyzed the results of *Wieczorek and Phillips* [2000] and showed that such models also predict large gravity or topography anomalies and electrical conductivity signatures that may be inconsistent with observations.

[10] In this study, we use 3-D thermochemical convection models to determine the consequences of KREEP localization in the PKT and compare these results with observations. Predictions are made that help determine if our current view of the PKT fits with the available data. In addition to previous models, we also calculate core temperatures and obtain core-mantle boundary heat flow estimates that can be used to test the origin and timing of a lunar dynamo. We also calculate surface gravity anomalies that can be compared with orbital observations. In section 2, we present the details of the thermochemical convection model we use and describe the model's initial conditions. In section 3, the results are first tested against previous models and observables, and then new consequences are presented. Finally, the results are discussed in section 4.

2. Model

[11] The thermal evolution of the Moon is studied using a thermochemical convection model for a fluid with a temperature-dependent viscosity in a spherical shell. We consider both core cooling and time-dependent radioactive decay as heat sources. In this section, we present the equations to be solved followed by a description of the initial conditions that we used in our simulations.

2.1. Convective Thermochemical Evolution Modeling

[12] When subjected to stress, planetary mantles behave as fluids on geological timescales. Their evolution is described by the general Navier-Stokes equations supplemented by suitable assumptions. In particular, for a fluid dominated by diffusion creep (i.e., Newtonian), with an infinite Prandtl number and within the Boussinesq approximation, the nondimensional equations for the conservation of mass, momentum, and energy are written as follows:

$$\nabla \cdot \vec{u} = 0, \tag{1}$$

$$-\nabla p + \nabla \cdot [\eta(\nabla \vec{u} + (\nabla \vec{u})^T)] + (TRa + CRa_C)\vec{e}_r = 0, \tag{2}$$

$$\left(\frac{\partial}{\partial t} + \vec{u} \cdot \nabla\right) T = \nabla^2 T + Q - L\frac{\partial F}{\partial t}, \tag{3}$$

where $\vec{e}_r$ is the radial vector, $\vec{u}$ is the velocity, p is the dynamic pressure, η is the viscosity, Ra_T and Ra_C are the thermal and compositional Rayleigh numbers, respectively, t is the time, T is the temperature, Q is the internal heat production rate, L is the latent heat of melting, F is the partial melt fraction, and C is the depletion field, which tracks the chemical properties of the material and which corresponds to the cumulated melt fraction. We use the assumption of Newtonian flow (as has been used in other studies, such as *Konrad and Spohn* [1997], *Spohn et al.* [2001], *Stegman et al.* [2003], and *Ziethe et al.* [2009]), but we note, as previously noted by *Christensen* [1984], that the effect of non-Newtonian rheology could be important, especially at low stresses.

[13] The diffusion creep viscosity η, normalized by η_0 can be written in nondimensional form as follows [*Roberts and Zhong*, 2006]:

$$\eta(T) = \exp\left(\frac{E}{T + T_{\text{surf}}} - \frac{E}{T_0 + T_{\text{surf}}}\right), \tag{4}$$

where E is the activation energy, T_{surf} the surface temperature, and T_0 the reference temperature, at which $\eta = \eta_0$. Assuming dry olivine dominates mantle rheology, we use a reference viscosity of 10^{21} Pa s at 1600 K [*Karato and Wu*, 1993]. Every quantity in the above four equations is nondimensional and the nondimensionalization factors can be found in Table 1. We also assume that the viscosity dependence on composition and melt fraction is negligible to first order. For computational purposes, the viscosity is limited to a maximum value of $\eta = \eta_{\max}$, where $\eta_{\max}$ is taken such that the stagnant lid regime is reached, i.e., the viscosity is high enough so that the crust is no longer mobile. The Rayleigh numbers are given by

$$Ra_T = \frac{\alpha_0 g_0 \rho_0 \Delta T D^3}{\kappa_0 \eta_0}, \tag{5}$$

$$Ra_C = \frac{g_0 \Delta \rho D^3}{\kappa_0 \eta_0}, \tag{6}$$

where α_0 is the reference thermal expansivity, g_0 the surface gravity acceleration, ρ_0 the reference density, ΔT the initial temperature drop across the mantle, D the mantle thickness, κ_0 the reference thermal diffusivity, and $\Delta\rho$ is the density change upon 30% mantle depletion, corresponding to the change from peridotite to harzburgite [*Scott and Stevenson*, 1989]. The two Rayleigh numbers arise in the adimensionalization process from the fact that the density is a function of temperature through thermal expansion and of the local depletion C, i.e.,

$$\rho = \rho_0 \left[1 - \alpha(T - T_0) - \frac{\Delta\rho}{\rho_0}\frac{C}{C_0}\right], \tag{7}$$

Table 1. Model Parameters

Symbol	Description	Value	Scaling
R_p	Planet radius	1740 km	$R_p - R_c$
R_c	Core radius	390 km	$R_p - R_c$
D_c	Crustal thickness	40 km	$R_p - R_c$
D_K	KREEP layer thickness	10 km	$R_p - R_c$
T_{surf}	Surface temperature	250 K	ΔT
T_0	Reference temperature	1600 K	ΔT
η_0	Reference viscosity	10^{21} Pa s	η_0
$\eta_{\max}$	Maximum viscosity	10^{28} Pa s	η_0
E	Activation energy	3 10^5 J mol^{-1}	$R\Delta T$
L	Latent heat of melting	6 10^5 J kg^{-1}	$c_p \Delta T$
R	Universal gas constant	8.314 J mol^{-1} K^{-1}	-
c_p	Mantle specific heat capacity	1000 J kg^{-1} K^{-1}	c_p
k_c	Crust thermal conductivity	1.5 W m^{-1} K^{-1}	k_m
k_m	Mantle thermal conductivity	3 W m^{-1} K^{-1}	k_m
κ_0	Reference thermal diffusivity	10^{-6} m^2 s^{-1}	$k_m/(\rho_0 c_p)$
ρ_0	Reference density	3400 kg m^{-3}	ρ_0
α_0	Thermal expansivity	2 10^{-5} K^{-1}	α_0
$c_{p,\text{core}}$	Core specific heat capacity	800 J kg^{-1} K^{-1}	c_p
ρ_{core}	Core density	7400 kg m^{-3}	-
k_{core}	Core thermal conductivity	25-50 W m^{-1} K–1	-
α_{core}	Core thermal expansivity	10^{-4} K^{-1}	-
ΔT	Temperature drop across the mantle	1750 K	-
$\Delta\rho$	Density difference between peridotite and harzburgite	60 kg m^{-3}	-
C_0	Melt fraction required between peridotite and harzburgite	0.3	-
Q_m	Radiogenic heating	cf. Table 2	$k_m/(D^2\rho_0)$
g	Surface gravity acceleration	1.62 m s^{-2}	g_0
Ra	Reference thermal Rayleigh number	2.24 10^5	-
Ra_C	Reference chemical Rayleigh number	2.4 10^5	-

where C_0 is the depletion required to obtain harzburgite. The depletion field models the current chemical state of the material and is calculated using the following transport equation:

$$\frac{\partial C}{\partial t} + \vec{u} \cdot \nabla C = \frac{\partial F}{\partial t}. \tag{8}$$

As for the temperature-induced density anomalies, the Boussinesq approximation requires density variations due to depletion to be small with respect to the background density. We note also that gravity is assumed constant in the mantle, which will tend to overestimate buoyancy effects at the core-mantle boundary. Consumption of latent heat through melting is taken into account by a sink in the energy equation [*Ita and King*, 1994], where we assume a linear consumption of latent heat with melt fraction (see equation (3)). Although melt transport is not directly taken into account, melt is assumed to leave the system instantaneously, thus, no latent heat is released when the system cools down. The melt is assumed to rise vertically, and the total amount of melt generated below each element on the surface is tracked as a function of time. For simplicity, we do not fractionate heat-producing elements into the melt. For low degrees of melting [*de Smet et al.*, 1999], the melt fraction can be written as

$$F = \frac{T - T_{\text{sol}}}{T_{\text{liq}} - T_{\text{sol}}}. \tag{9}$$

[14] This convective thermochemical modeling approach has been widely used [*Konrad and Spohn*, 1997; *Spohn et al.*, 2001; *Ziethe et al.*, 2009] and discussions about mantle composition are postponed to section 4. We assume here a peridotite composition with solidus and liquidus of KLB-1 peridotite from *Hirschmann* [2000]:

$$T_{\text{sol}} = 1409 + 134.2P - 6.581P^2 + 0.1054P^3, \tag{10}$$

$$T_{\text{liq}} = 2035 + 57.46P - 3.4872P^2 + 0.0769P^3, \tag{11}$$

where P is the hydrostatic pressure in GPa. The effect of an insulating crust is also taken into account by assigning a lower thermal conductivity to the crust. Here we assume a constant thickness of 40 km [*Khan and Mosegaard*, 2002; *Lognonné et al.*, 2003; *Wieczorek et al.*, 2013] and a thermal conductivity of k_c = 1.5 W m^{-1} K^{-1} in order to account for the presence of low-conductivity megaregolith. This value has been estimated from the case where ∼5 km of megaregolith with k_r = 0.3 W m^{-1} K^{-1} is on top of 35 km of crust with k_c = 3 W m^{-1} K^{-1}. All model parameters and their nondimensionalization are described in Table 1.

[15] We solve the set of equations (1)–(3) in a 3-D spherical geometry using the finite-volume convection code Gaia, which has already been validated in other publications [e.g., *Hüttig and Stemmer*, 2008] and which can accurately handle localized viscosity variations of up to several orders of magnitude. Equation (8) is solved using a tracer approach using 20 particles per cell [e.g., *van Keken et al.*, 1997], and whose implementation in Gaia has been extensively tested by *Plesa et al.* [2013]. This tracer approach essentially eliminates numerical diffusion and allows us to treat accurately sharp composition contrasts and to resolve subgrid structures. Our simulations were carried out using a 20 km radial and a 60 km lateral resolution. The boundary conditions are free slip both at the surface and core-mantle boundary. The surface temperature is fixed at 250 K while the core-mantle boundary temperature is decreasing as the core cools. The core in

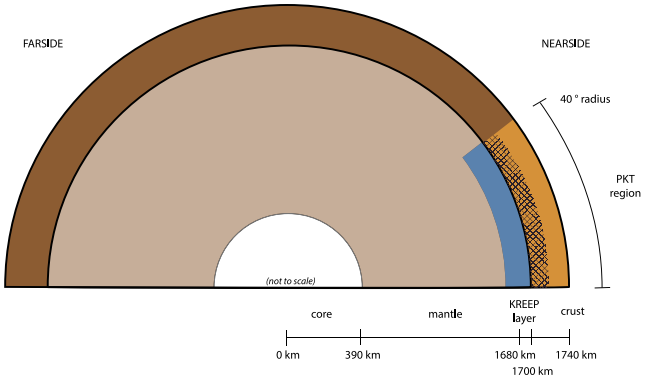

Figure 2. Schematic diagram of the thermochemical convection model setup (not to scale). The equivalent of 10 km of KREEP basalt is placed below a 40 km thick crust (blue), in the lower 20 km of the crust (cross hatch), or redistributed over the entire crust (orange). The lateral extent of the PKT is 80° in diameter and the radial resolution is 20 km. The temperature of the core T_c evolves with time, but does not include the energetics of core crystallization.

our model acts as an isothermal heat bath, whose cooling depends on its density and heat capacity (Table 1). Given the high viscosity of the surface, its velocity is negligible, and the assumption of a no-slip surface has no effect on the results. A schematic of the model geometry can be found in Figure 2. For comparison with our convection results, we also ran a set of simulations that are purely conductive.

2.2. Initial Conditions

2.2.1. Heat Sources

[16] Whether the Moon possesses a composition in refractory elements similar to the Earth or is enriched by a factor of about 2 is a long-lasting debate [*Taylor*, 1982; *Warren*, 2001; *Taylor et al.*, 2006]. This is critical for thermal evolution models of the Moon, as the bulk abundance of uranium is estimated to range from 17 ppb for primitive Earth values to 34 ppb in the enriched case.

[17] The abundance of heat-producing elements in the lunar mantle can be estimated from the composition of primary mantle melts and mineral/melt partition coefficients. As the most primitive primary melts, the picritic glasses, have a large range of compositions, different authors have advocated different values for the bulk mantle composition. We consider two representative numbers: 25 ppb thorium from *Warren and Wasson* [1979] and 40 ppb thorium from *Jolliff et al.* [2000]. We estimate the present-day mantle abundance of U and K using an average Th/U ratio of 3.7 and a K/U ratio of 2500 [*Taylor*, 1982].

[18] Our model contains a layer of KREEP-rich material that is concentrated in the Procellarum KREEP Terrane (PKT). We note simply that if a global 2 km KREEP layer (as was once envisioned during the Apollo era [*Warren and Wasson*, 1979]) was segregated beneath the PKT, such a layer would be about 10 km thick. We thus assume that the KREEP layer is 10 km thick, as in *Wieczorek and Phillips* [2000], but acknowledge that its true thickness is somewhat uncertain. We choose the uranium concentration of this layer to be 3.4 ppm, which corresponds to the average uranium content of Apollo 15 KREEP basalts [*Korotev*, 2000]. Though KREEP basalts are rare in the Apollo sample collection, this composition is representative of a large portion of the materials that were excavated by the Imbrium impact basin, which lies within the PKT. Because the radial resolution of our model is 20 km, when the KREEP layer is thinner than this, we place the equivalent amount of heat-producing elements in a 20 km thick layer.

[19] We model the KREEP layer as a cylindrical cap of either 40° or 80° diameter and the equivalent of 10 km KREEP basalt is placed either below the crust, at the bottom of the crust, or redistributed over the entire crust (see Figure 2). When the KREEP layer is redistributed over the entire crust, the resulting concentration is obtained from mass conservation. The crustal regions that are not enriched in heat sources have a uranium concentration of 0.14 ppm [*Jolliff et al.*, 2000], which is consistent with a viscoelastic study of lunar impact basins deformations that suggests that the farside crust is more than 10 times depleted in heat sources with respect to the PKT region [*Kamata et al.*, 2013].

[20] The KREEP layer is not fixed to its initial position and is free to flow with time. When the KREEP layer is placed within the mantle, we assume that its density is equal to that of the surrounding mantle, even though the Mg-rich composition of KREEP basalt implies a density that is lower than typical mantle materials. Since our KREEP layer is only one grid element thick, we have run higher-resolution simulations in 2-D with a 5 km radial resolution to better quantify how this material is displaced with time. Our results show that only a very small portion of the KREEP layer at its edge gets entrained into the mantle flow, and we thus expect that our poor resolution of the KREEP layer will not have any significant influence on the results.

[21] Our assumed distribution of heat sources leads to extreme cases with bulk uranium contents between 19.6 ppb for a 40° diameter PKT and a mantle with the lowest concentration of uranium, and 28.7 ppb for an 80° diameter PKT and the highest concentration of uranium in the mantle. The bulk compositions lie well within the Earth-like and enriched scenarios discussed above. Our preferred model has an 80° diameter PKT, a mantle with the most depleted concentrations, and a KREEP layer emplaced below the crust. For this model, the bulk uranium concentration is 19.6 ppb, which is similar to the value for the bulk silicate Earth, and which is consistent with recent bulk Moon composition estimates derived from the GRAIL mission [*Wieczorek et al.*, 2013]. This corresponds to having about one third of the Moon's heat sources in the PKT region. A summary of the heat-source concentrations can be found in Table 2.

2.2.2. Initial Temperature Profile

[22] To cover the range of possible Moon formation and initial differentiation scenarios, we considered a range of initial temperature profiles. Every profile starts initially from a surface temperature of 250 K at 4.5 Ga and ends at a value of 2000 K at the core-mantle boundary in order to account for an excess temperature in the core due to differentiation of several hundred degrees [*Konrad and Spohn*, 1997]. The core is then allowed to cool as an isothermal heat bath. The choice of the temperature increase with depth in the mantle is then linked to an assumed magma ocean crystallization scenario. The dynamics of such a system are complex, and

Table 2. Uranium Concentration for the Different Model Layers[a]

Model	PKT Diameter	Mantle ppb	KREEP ppm	Enriched Crust ppm	Crust ppm	Bulk Silicate Moon ppb
0LB[b]	80°	6.8[c]	3.4[d]	-	0.14[e]	25.1
1LB	80°	10.8[e]	3.4	-	0.14	28.7
0SB	40°	6.8	3.4	-	0.14	19.7
1SB	40°	10.8	3.4	-	0.14	23.4
0LD	80°	6.8	3.4	-	0.14	24.5
1LD	80°	10.8	3.4	-	0.14	28.2
0SD	40°	6.8	3.4	-	0.14	19.6
1SD	40°	10.8	3.4	-	0.14	23.3
0LW	80°	6.8	-	0.82[f]	0.14	25.1
1LW	80°	10.8	-	0.82	0.14	28.7
0SW	40°	6.8	-	0.82	0.14	19.7
1SW	40°	10.8	-	0.82	0.14	23.4

[a]For all cases, K/U = 2500 and Th/U = 3.7 [*Taylor*, 1982]. In this table, "KREEP" refers to the 10 km layer below the crust, "enriched crust" refers to the case where the KREEP layer is redistributed over the entire crust, and "crust" refers to the unenriched part of the crust. "0" and "1" refer to the mantle heat source content, "0" being the lowest and "1" the highest. "L" and "S" refer to the PKT diameter (i.e., large and small). "B," "D," and "W" correspond to the KREEP emplacement geometry: below the crust, distributed at the bottom of the crust, or within the entire crust, respectively.
[b]Preferred model.
[c]*Warren and Wasson* [1979].
[d]*Korotev* [2000].
[e]*Jolliff et al.* [2000].
[f]From mass conservation.

we therefore consider two extreme cases. The "cold" case assumes an adiabatic gradient within the whole mantle [as in *Wieczorek and Phillips*, 2000] corresponding to a well-mixed, initially convecting interior. We note that as gravity is assumed constant as a function of depth, we slightly overestimate the adiabatic gradient. The temperature profile of the "hot" case follows the mantle solidus for the first 700 km, below which the mantle is adiabatic. For this scenario, the region at the solidus represents the upper portion of the solidified magma ocean that did not convectively readjust. In both cases, the initial temperature profile is linear in the crust, reaching the mantle solidus at the crust-mantle interface. Our preferred case ends up having an intermediate profile, following the solidus down to 350 km depth (Figure 3). We do not consider stable post-magma ocean overturn temperature profiles here [such as in *Hess and Parmentier*, 1995; *Elkins-Tanton et al.*, 2011], in an attempt to keep the setting of our model as simple as possible. We note simply that if there were any density gradients with depth, that this would limit the amount of convection, and that the thermal evolution would approach a model that was purely conductive [as in *Wieczorek and Phillips*, 2000].

3. Results

[23] Before describing our simulation results, we describe the conditions that we consider consitute a successful model. First, a successful model must give rise to volcanism primarily within the PKT, and only a small amount exterior to this region and on the farside. Second, mare volcanism must last for a significant amount of time, from > 4 Ga to about 1 Ga. Third, the total volume of extrusive lava flows has been estimated to lie between $2 \cdot 10^6$ and $7 \cdot 10^6$ km^3 [e.g., *Wieczorek et al.*, 2006; *Shearer et al.*, 2006]. If the ratio of intrusive to extrusive magmatism is 5 : 1 [*White et al.*, 2006], then the total volume of generated magma should lie somewhere between $1.2 \cdot 10^7$ and $4.2 \cdot 10^7$ km^3. Given that the intrusive to extrusive ratio is not known with any certainty and that the thicknesses of the mare are also uncertain, this estimate should be considered uncertain by a factor of about 5. Fourth, based on the ages of mare basalts in Figure 1, the youngest lavas should erupt in the center of the PKT. Finally, the surface heat flow must be compatible with the measurements made at the Apollo 15 and 17 landing sites.

3.1. Thermal Evolution

[24] Our nominal model (model "0LB," see Table 3) started with an intermediate initial temperature profile, with the KREEP layer located below the 40 km thick crust,

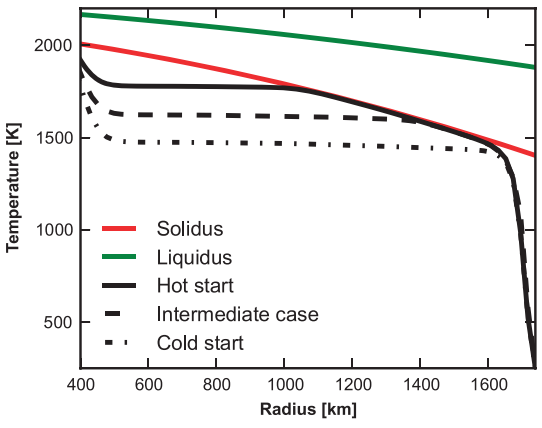

Figure 3. Initial temperature profiles. For all models the temperature at the crust-mantle interface is set to the solidus of the mantle. The cold case starts with an adiabatic gradient in the mantle, the intermediate case follows the mantle solidus down to 350 km and is adiabatic below, and the hot case follows the mantle adiabat to 700 km and is adiabatic below. Our preferred model corresponds to an intermediate case following the solidus down to 350 km depth (see text for details). Solidus and liquidus are taken from *Hirschmann* [2000].

Table 3. Models Summary Including the Main Melting Characteristics[a]

	Nearside			Farside		
	Duration of Melting	Max Depth	Total Vol.	Duration of Melting	Max Depth	Total Vol.
Model	Ga	km	km^3	Ga	km	km^3
I-0LB	4.5–0.2	660	3.7e8	3.8–3.1	680	3.5e7
I-0LD	3.8–2.5	700	5.2e7	3.8–3.1	680	2.5e7
I-0LW	3.8–1.6	700	7.5e7	3.8–3.0	680	2.5e7
H-0LB	4.5–0.0	980	6.7e8	4.1–1.6	990	4.3e8
H-0LD	4.3–0.6	880	7.0e8	4.3–1.6	860	6.6e8
H-1LW	4.3–0.0	1150	1.4e9	4.3–0.0	1160	1.2e9
C-0LD	-	-	-	-	-	-
C-0LB	4.5–0.4	540	1.6e8	-	-	-
C-1LW	2.6–0.5	800	2.0e8	1.3–1.1	770	2.7e4

[a]"I," "C," and "H" correspond to intermediate, cold, and hot initial temperature profiles, respectively. The rest of the nomenclature is the same as in Table 2.

and has Earth-like bulk abundances of refractory elements. About one third of the heat source budget concentrated in a small region on the nearside hemisphere, and as shown in Figure 4 as a series of temperature slices, this has a dramatic influence on the thermal history of the Moon. Other examples of thermal evolutions can be found in Figures 10–12. Contrary to thermal evolution models with a symmetric distribution of heat sources, where the global cooling rate dictates the mantle behavior, the PKT region is the driver in our case as it heats the underlying mantle. This is not a new result [e.g., *Wieczorek and Phillips*, 2000], but contrary to previous conductive models that studied the

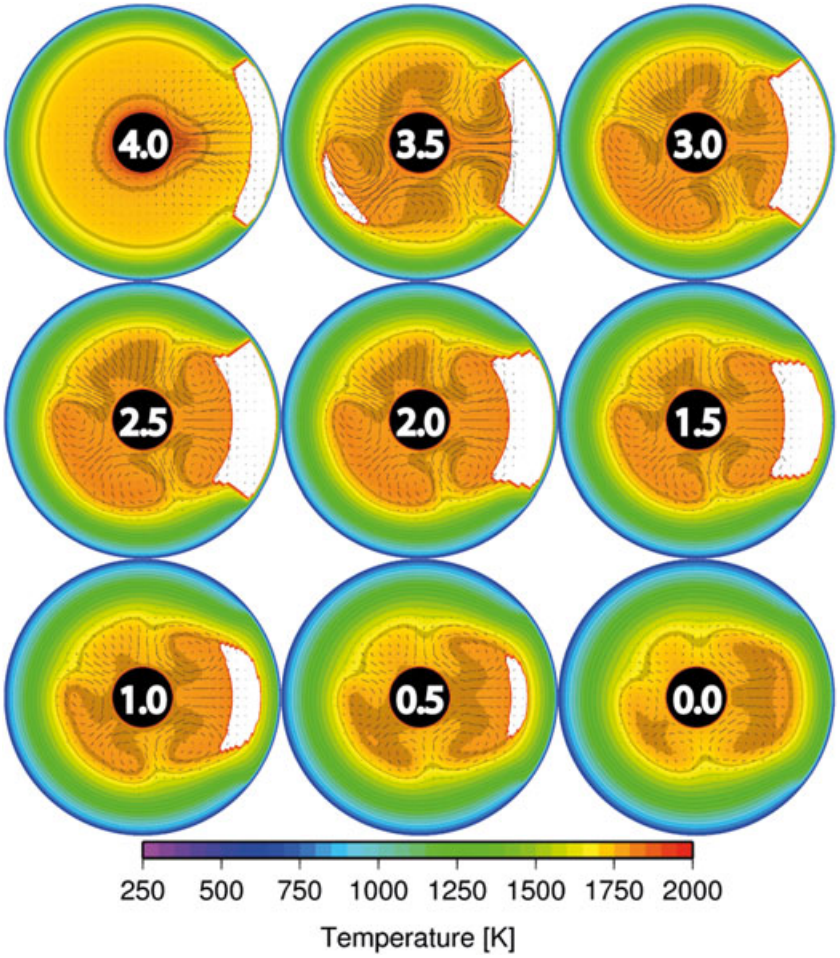

Figure 4. Temperature cross sections of the lunar mantle for a complete thermal evolution for the case with an intermediate initial temperature profile and the KREEP layer located below the crust (model "T-0LB"). Numbers correspond to time before present in Ga. The black circle is the lunar core and white corresponds to regions that are partially molten. The streamlines are shown as dashed lines.

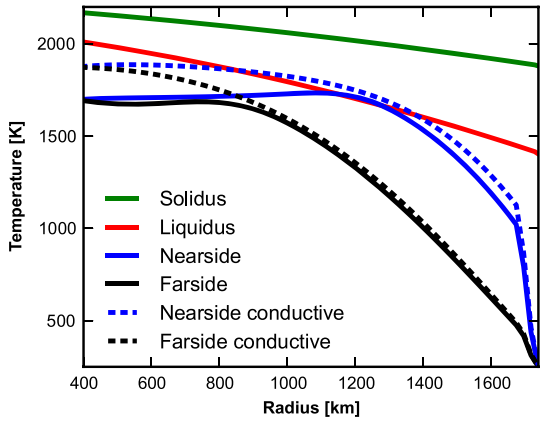

Figure 5. Present-day temperature profiles beneath the center of the PKT and beneath the center of the farside (solid lines) for our preferred case (model T-0LB) compared with the results of a purely conductive simulation (dotted).

PKT, our simulations show that heating of the underlying mantle helps develop a stronger convection in the nearside mantle than in the farside. As shown in Figure 5, this leads to a more efficient cooling than would occur in a purely conductive model. For a description of symmetrical lunar thermal evolutions models, the reader is referred to *Spohn et al.* [2001] and *Ziethe et al.* [2009].

[25] Figure 6 shows how the present-day heat flux varies as a function of distance from the center of the Procellarum KREEP Terrane. In the center of the PKT, we find a maximum value of about 25 mW/m^2 and a background value outside of this terrane of about 10 mW/m^2. These values are similar to the measurements made at the Apollo 15 and 17 landing sites, i.e., 21 $\pm$ 3 and 14 $\pm$ 2 mW/m^2, respectively [*Langseth et al.*, 1976], especially when considering that the precise locations of these landing sites with respect to the edge of the PKT are somewhat uncertain. As a result of lateral variations in megaregolith thickness [*Warren and Rasmussen*, 1987], the Apollo heat flow estimates should perhaps be corrected downward to 18 and 12 mW/m^2. As shown in Figure 7a, the heat flux in the PKT is predicted to be about a factor of 2 greater than that in the surrounding highlands during most of the Moon's thermal evolution. The present-day heat flux is found to be rather insensitive to the various initial conditions that were considered (Figure 6).

[26] The high concentration of heat sources in the PKT leads to nearly instantaneous partial melting of the underlying mantle. For this reference model, after about 600 million years, melting is also observed on the farside, but lasts for only a few 100 million years. The time at which farside melting occurs is related to the time to initiate global convection, and hence is directly related to the Rayleigh number [e.g., *Schubert et al.*, 1969]. On the nearside, the region where melt occurs increases with depth over time, reaching 600 km after 2 billion years. Afterward, this region starts to shrink, with the last magmas being confined to depths of about 500 km a few 100 million years before present. The PKT-induced mantle circulation on the nearside produces two slowly convecting cells that bring down cold materials approximately 80° away from the center of the PKT at about 0.25 cm/yr. Overall, mantle remixing is inefficient, with velocities below the lithosphere reaching 0.2 cm/yr on average on the nearside and 0.15 cm/yr on the farside 3.5 Ga ago, decreasing to about 0.05 cm/yr at the present day. This is an order of magnitude slower than on the Earth with velocities estimated from sinking slabs [e.g., *van der Meer et al.*, 2009] and corresponds to about one complete overturn of the lunar mantle in 4.5 billion years. As a result, even when KREEP is emplaced below the crust, with the same density as the mantle, it is dynamically stable over the whole evolution of the Moon.

[27] We estimate the average change in radius of the Moon on its nearside and farside hemispheres due to the changes in density that occur from thermal expansion and compositional depletion. The estimated change of radius from mapping of contractional and compressional features takes only into account changes since the end of basin formation at about 3.8 Ga. As shown in Figure 7b, up to 7 km of expansion occurs on the nearside during the first 600 million years, but surface expressions from this epoch are not expected to be seen today. Since 3.8 Ga, about 1 km of expansion occurred on the nearside until about 3 Ga, at which point contraction started to dominate. A present-day total contraction of about 2 km is expected to be seen on the nearside (Figure 7b). In contrast, on the farside, contraction is found to be continuous throughout lunar history and produces a present-day contraction of about 3 km. The presence of an early period of expansion on the nearside is in agreement with what appear to be giant magmatic dikes, as observed in the GRAIL data by *Andrews-Hanna et al.* [2013]. However, as their model requires global expansion to account for similar features on the farside hemisphere, this is not compatible with our model results which show that the farside hemisphere was always contracting. Finally, our

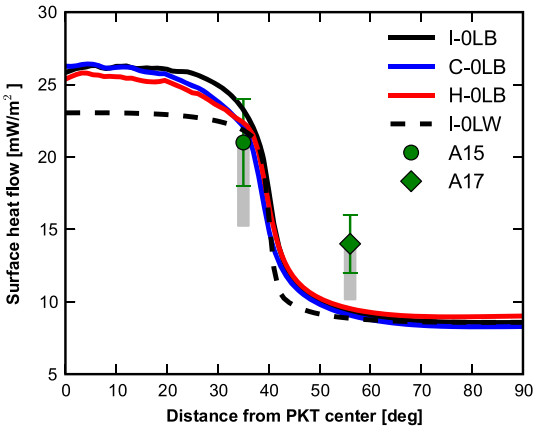

Figure 6. Average surface heat flow as a function of distance from the center of the PKT for several simulations. The solid lines correspond to cases where KREEP is emplaced below the crust and the dotted line when it is redistributed within the entire crust. "C-," "I-," and "H-" correspond to cold, intermediate, and hot initial temperature profiles. The nomenclature follows Table 3. The green dot and diamond are the surface heat flow estimates at the approximate locations of the Apollo 15 and 17 landing sites, respectively [*Langseth et al.*, 1976], and the gray boxes include the correction due to heat flow focusing from *Warren and Rasmussen* [1987].

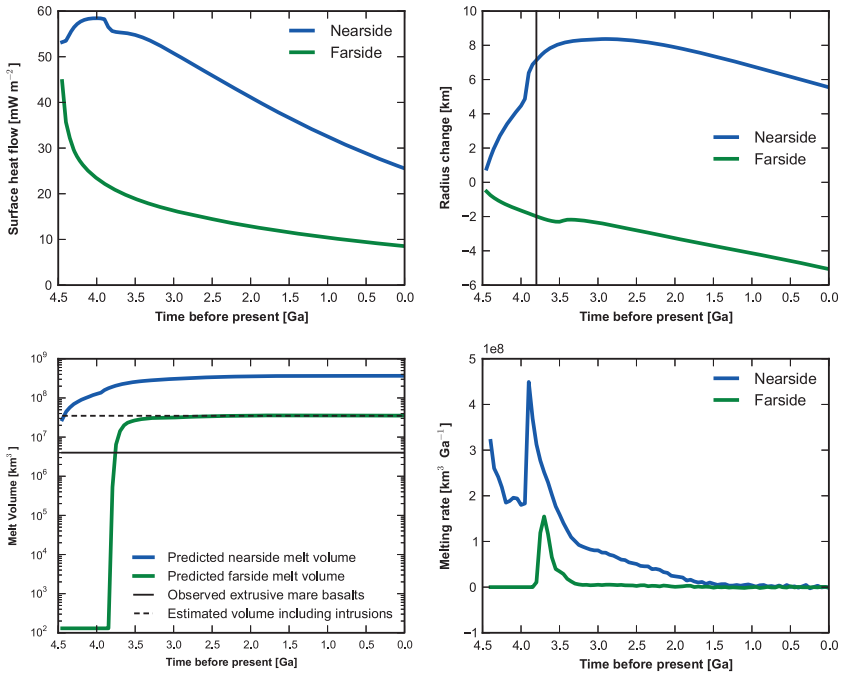

Figure 7. (a) Surface heat flow in the center of the PKT and on the farside as a function of time before present. (b) Radius change in the center of the PKT and farside due to secular cooling as a function of time before present. The vertical line denotes the approximate end of the putative late heavy bombardment. (c) Cumulate melt volume averaged over the nearside and farside (solid lines). Total mare basalt volume estimate (thin black line) is from *Shearer et al.* [2006], and the maximum melt volume (dashed line) takes into account a 5 : 1 intrusive to extrusive volcanism ratio [*White et al.*, 2006]. (d) Average melt production rate on the nearside and farside. These figures were obtained for our preferred case (model T-0LB).

predicted contraction on the nearside is in agreement with the global value of about 1 km estimated by *Watters et al.* [2010], but continuous contraction of the farside leads to a much larger change in radius than is implied by the observed contractional features. Nevertheless, these authors state that their estimate is a lower limit and may be uncertain by a factor of about 2.

[28] We ran a series of simulations varying the heat source content and distribution, the size of the PKT and the initial temperature profile (see Table 3 for a summary and Figures 10–12 for examples of thermal evolutions). Three major consequences always arise from the initial hypothesis of localized heat sources. First, melt is localized on the nearside while the farside remains mostly undisturbed by the PKT. The amount of farside melting is highly dependent on the mantle's initial temperature profile. Second, a thermal anomaly is preserved until the present day in the mantle underlying the PKT. And third, the asymmetric heating from the PKT has an influence down to the core-mantle boundary. The consequence of these results are described in more detail in the following subsections, with an emphasis placed on understanding the general attributes of models with an enhancement of heat production in the Procellarum KREEP Terrane, and not models that fit a specific observation exactly.

3.2. Magmatism

[29] The main influence on the Moon's magmatic history is the assumed initial temperature profile. A higher initial temperature leads to more melting, as expected, but also to earlier and deeper melting. This is a very strong constraint, as models with a cold initial temperature profile fail to produce any significant amount of melt on the farside. On the other hand, the hot initial start tends to produce too much melting (on the order of 10^9 km^3 on the farside alone). As discussed later, the assumed solidus for the mantle has a large influence on the total volume of magma that is generated as well, but this (and the mantle composition) is poorly constrained.

[30] The exact emplacement and configuration of the KREEP layer does not have much influence on the farside evolution, but it does have a strong influence on the nearside magmatic history. When the KREEP layer is emplaced below the crust, melting starts immediately and stops a few hundred million years ago for all models, independently of the initial temperature profile. The influence of the initial temperature profile simply reflects the maximum depth of melting. While the hot model produces melt down to about 1000 km, the intermediate and cold cases reach 600 and 500 km depth, respectively. When the KREEP layer is initially evenly redistributed in the entire crust, it has a smaller effect on the mantle as heat is lost more easily to space. In this case, the melting duration and depth are highly dependent on the initial temperature profile: a hot initial temperature profile leads to melting at greater depths, but also to a longer duration than for a cold initial start. The case where the KREEP layer is emplaced in the lower portion of the crust is very similar to the case where it is redistributed in the entire crust: the exact melting time and volume is subject to a trade-off between initial temperature and bulk heat sources content.

Nevertheless, none of the models that we explored with a KREEP layer either redistributed within the entire crust or emplaced at the bottom of the crust succeeded in matching the estimated timing and amount of volcanism on the nearside (see Table 3 for a summary and Figure 13 for a comparison). Under the assumptions of our modeling, this suggests that KREEP was most probably emplaced below the crust.

[31] The model that best fits the estimates of nearside and farside volcanism corresponds to an intermediate temperature profile with the KREEP layer emplaced directly below the crust (model "T-0LB" in Table 3). As shown in Figure 7, melting then occurs on the nearside from 4.5 to 0.2 Ga ago, reaches about 600 km depth below the PKT and generates about $5 \cdot 10^8$ km^3 of magma with a peak in magma production between 4 and 3.5 Ga ago. Consistent with observations (Figure 1), the youngest lavas are found to erupt in the center of the PKT. Farside melting is characterized by a main volcanic phase starting 3.7 Ga ago that generates $2 \cdot 10^7$ km^3 of magma (see Figure 7 for details). For this particular model, about 10 times more melt is produced on the nearside than on the farside, consistent with current estimates [*Wieczorek et al.*, 2001; *Morota et al.*, 2009].

[32] If all the generated magma was assumed to erupt onto the surface, the thickness of the lava flows would be on average about 30 km on the nearside and 10 km on the farside. However, if we assume an intrusion to extrusion ratio of 5, these thicknesses would be reduced to 5 and 1.7 km, respectively. The estimated thickness of mare basalts vary from a few hundred meters to several kilometers in large basins [*Williams and Zuber*, 1998]. The averages that we find for our nominal model are therefore probably a factor of 2 to 5 too large. Nevertheless, we note that our simulations will tend to overestimate the amount of melting, as discussed in section 4, because the increase in temperature of the solidus with mantle depletion is not considered in our models, nor is the fractionating of heat producing elements into the magma considered. Considering these uncertainties, we find the model we show in Figure 7 to be largely compatible with the observations.

[33] The bulk composition of the Moon is a long-standing debate. It was first argued to be enriched in refractory elements in comparison to the Earth [*Taylor*, 1982]. With revised estimates of the surface heat flow, *Warren and Rasmussen* [1987] claimed that the bulk composition could be similar to that of the primitive Earth. We find that to stay within observational constraints on the volume of mare basalts and the timing of mare volcanism, the lower bulk heat source contents are preferable, which is consistent with the latest view of an Earth-like composition for the Moon [*Wieczorek et al.*, 2013].

3.3. Predicted Gravity Field

[34] For acceptable models, mantle melting should be almost over today as no present-day volcanism is observed. Nevertheless, even though melting ceases before the present, we always observe a temperature anomaly below the PKT, and this has direct consequences on the Moon's global gravity field. We calculate the predicted radial gravity anomalies, g, using the spherical harmonics expansion:

$$g(r,\theta,\phi) = \frac{GM}{r^2}\sum_{l=0}^{\infty}\sum_{m=-l}^{l}\left(\frac{R_0}{r}\right)^l (l+1)C_{lm}Y_{lm}(\theta,\phi), \qquad (12)$$

where r, θ, and ϕ are the coordinates of observation, G is the gravitational constant, M the mass of the Moon, R_0 the reference radius of the spherical harmonic coefficients C_{lm}, and Y_{lm} the spherical harmonic functions of degree l and order m [e.g., *Wieczorek*, 2007]. The radial gravity anomalies are positive when directed downward. The spherical harmonic coefficients C_{lm} have contributions from several sources, such as buoyancy generated by temperature and compositional variations, thermal uplift of the surface, and the extruded mare basaltic lava flows.

[35] For the temperature and compositional contributions, the spherical harmonic coefficients of the gravitational field are obtained by integrating the contributions of a large number of thin spherical shells:

$$C_{lm} = \frac{4\pi}{M(2l+1)}\sum_{i=1}^{N} r_i'^2\left(\frac{r_i'}{R_0}\right)^l \rho_{lm}(r_i')\Delta R, \qquad (13)$$

where $\rho_{lm}(r)$ are the spherical harmonics coefficients of the density distribution at radius r. For all the following calculations, we removed the degree-0 coefficient, which corresponds to a globally constant gravitational contribution. As shown in Figure 8a, the contribution to the gravity field from temperature induced lateral variations in density is maximal in the center of the PKT and has a value of about –500 mGal using a thermal expansion coefficient of $2 \cdot 10^{-5}$ K^{-1}. As can be seen in the temperature-density relation of equation (7) and the linearity between density and gravity in equation (13), the magnitude of this gravity anomaly is linearly related to the thermal expansivity α. If we were to have used $\alpha = 3 \cdot 10^{-5}$ K^{-1}, as in *Grimm* [2013], we would obtain a maximum value for the gravity anomaly of –800 mGal, consistent with his findings. In addition to this effect of temperature on the Moon's gravity field, partial melting of a peridotitic mantle leads to the formation of harzburgite residue with a lower density, which will influence the observed field as well. This density contribution is calculated using the chemical depletion part of equation (7). This contribution was neglected in the work of *Grimm* [2013], and we find that this compositional effect contributes an additional negative gravity anomaly of about –600 mGal (Figure 8b).

[36] In addition to the temperature and compositional contributions, a positive contribution from surface uplift will also occur. Under the assumption of a strengthless lithosphere, mantle flow driven by thermochemical density variations will produce surface deformation. Although this is not taken into account in our convection model explicitly, it can be estimated a posteriori using a well-established formalism [e.g., *Richards and Hager*, 1984]. The total predicted topography is found to be about 4.8 km (7.2 km when using $\alpha = 3{\cdot}10^{-5}$ K^{-1}), in close agreement with the prior estimate of *Grimm* [2013]. Using a modification of equation (13) [e.g., *Wieczorek*, 2007], we calculate in Figure 8c the gravity contribution of this surface relief to be +700 mGal. However, the presence of an elastic lithosphere could have a significant effect in reducing this dynamic topography [*Zhong*, 2002; *Golle et al.*, 2012]. If the lithosphere were perfectly rigid, there would be zero uplift, and hence there would be no positive gravity anomaly associated with the surface. The strengthless and rigid lithosphere scenarios represent two extreme scenarios that will bracket all intermediate cases. We note here that our case with a rigid lithosphere should

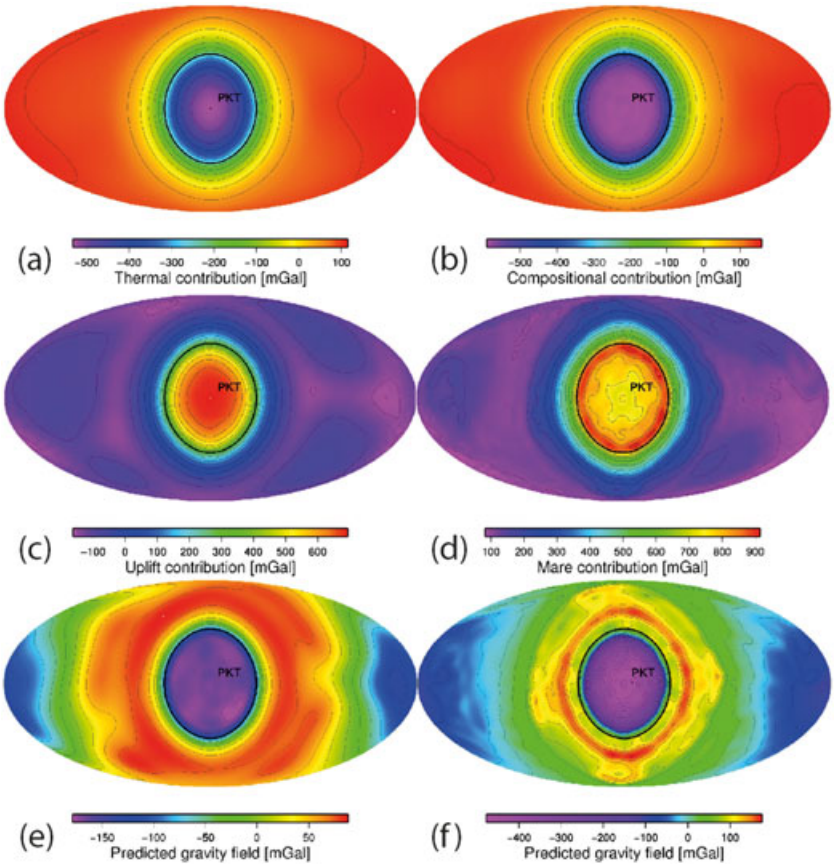

Figure 8. Gravity field of the Moon. Contributions from (a) thermal expansion, (b) compositional depletion in the mantle, (c) uplift of the surface for a strengthless lithosphere, and (d) uncompensated mare basalts with a maximum thickness of 5 km. For these contributions, the degree-0 term has been removed, but the degree-1 term is included. Predicted gravity anomaly (e) for a strengthless lithosphere with isostatically compensated mare basalts and (f) for a completely rigid lithosphere with uncompensated mare basalts and zero thermal uplift. For the last two figures, the degree-1 gravity field (which corresponds to change in the planets center of mass) has been removed. All figures are presented in a Mollweide equal-area projection centered on the PKT. The black circle corresponds to the extent of the PKT. The results are calculated for our preferred case (model T-0LB).

be treated with caution: In incompressible models, considering the effect of thermal expansion without including surface uplift in essence removes mass from the system.

[37] In this work, we do not perform the exact flexure calculation as there are several complications that would make this calculation highly uncertain. For example, a significant part of the load acting on the lithosphere comes from degree-0 and degree-1 terms, but these are not taken into account in standard spherical shell flexural models, such as those based on *Turcotte et al.* [1981]. Furthermore, the degree-0 term would act to place the lithosphere into extension or compression, which could give rise to fractures that would invalidate the spherical shell flexure formalism, and which would also set up in-plane forces that are not generally considered. Furthermore, the elastic thickness of the lithosphere is expected to vary laterally, which again would invalidate the assumptions of most simple elastic shell flexure models (though see *Beuthe* [2008]). As an example, if we take the 750 K isotherm as representing the elastic thickness of the lithosphere [*Watts and Zhong*, 2000], at 3.5 billion years ago during the main phase of mare volcanism, the elastic thickness is predicted to be less than 30 km in the PKT and 80 km for the farside highlands, consistent with estimates from *Crosby and McKenzie* [2005]. Finally, any flexure calculation would need to consider the load caused by the mare basalts and intrusive magmas, which are not well constrained.

[38] The final gravitational signature to consider is that due to the eruption of dense lavas onto the surface, and the formation of dense intrusions in the crust. The magnitude of this anomaly, however, will depend sensitively on their assumed compensation state. If the lithosphere attained a state of isostatic equilibrium, perhaps because of the temperatures associated with melting in the underlying mantle, the final gravity anomaly would be nearly zero. However, if the lavas were perfectly uncompensated, the gravity anomaly would be about +140 mGal for each km of uncompensated lava. If the mare basalts were about 5 km thick, as observed in the previous section, then this gravity anomaly could reach up to +700 mGal (Figure 8d). Considering the intrusive components would generate an even larger anomaly. Nevertheless, given that the mare does not possess distinct

gravity signatures (with the exception of mascon basins, see *Zuber et al.* [2013]), it is probable that the loads on the lithosphere resulting from intrusive and extrusive lavas are at least partially compensated. We note in addition that downward attenuation of the anomaly in equation (13) implies that the positive contribution from dense material taken from depth will be larger than its negative counterpart.

[39] In this paragraph, we present the total predicted gravity field corresponding to two extreme cases. We first assume that the lithosphere did not possess significant strength at the time of mare volcanism (i.e., the basalts are assumed to be compensated) and plot the total gravity anomaly in Figure 8e. For our final gravity map, we remove the degree-1 gravity signature, which corresponds to a slight change in the center of mass of the planet of about 1 km toward the nearside. The combined signal is seen to be small, with an anomaly of about –200 mGal within the PKT. If only about 1–2 km of basalts (or their intrusive equivalent) were partially uncompensated, the total gravity anomaly would be close to zero, consistent with the observations (the observed gravity anomalies in the PKT range from about –100 to 200 mGal, excluding the mascon basins). Second, if we assume that the lithosphere were completely rigid, the lack of thermal uplift in the PKT, combined with 5 km of uncompensated basalts, would generate an anomaly of –400 mGal, as shown in Figure 8f. If we were to include the gravity contribution from the uncompensated magmatic intrusions at the crust-mantle interface, the gravity anomaly could be as high as +3000 mGal, which tends to argue against the scenario of a rigid lithosphere. In conclusion, under reasonable assumptions, it is possible to find models that do not predict a large gravity anomaly to be present within the PKT.

[40] In contrast to the gravity field, our thermal model does predict surface topography that might be inconsistent with the observations. For example, the model presented in Figure 8e, where the lithosphere possesses no strength in the PKT, dynamic topography generated by thermal expansion in the underlying mantle predicts about 5 km of uplift [see also *Grimm*, 2013]. Since this model also generates a shift in the center of mass of about 1 km toward the nearside, this topographic uplift in the PKT should be reduced by the same amount. Still, given that the PKT is located in a region where the surface elevations are about 2 km below the average, this is a potentially discrepant model result. If, on the other hand, we assume that the lithosphere is perfectly rigid, there will be no topographic uplift in the PKT. This model predicts a change in the center of mass of about 2 km toward the farside hemisphere, which would result in an uplift of 2 km on the nearside, which is also inconsistent with the observations.

[41] The magnitude of our modeled contributions depends both on the depth and amplitude of the subsurface thermal anomaly as well as on the lithospheric thickness. Models where the KREEP layer is distributed within the crust lose more heat to space and therefore tend to produce a smaller thermal anomaly and surface uplift than models where the KREEP layer is emplaced below the crust. The model "T-0LW" for example predicts about 2.5 km uplift and surface gravity anomalies on the order of ±40 mGal. Similarly, a lower initial temperature model exhibits a smaller anomaly at the present day. Model "A-0LB" for example predicts gravity anomalies that are about 60% smaller than model "T-0LB."

[42] The most recent spacecraft observations show no significant gravity anomaly associated with Oceanus Procellarum, which suggests that it is probably regionally compensated [*Zuber et al.*, 2013]. The observed topography in the PKT, however, is negative, not positive as might be expected from thermal uplift. We offer two possible explanations for this apparent conundrum. First, if the low elevations of the nearside crust are a result of crustal thickness variations [*Wieczorek et al.*, 2013], this could easily mask the topographic signature of thermal uplift. Using a simple Airy isostasy model, a reduction in the crustal thickness by about 20 km would reduce the surface topography by 5 km. Second, since the high-titanium mare basalts erupted only on the nearside hemisphere, it is possible that the nearside mantle is denser than the farside because of its higher titanium content. This would give rise to a shift in the center of mass toward the nearside, which would reduce the nearside surface topography by the same amount.

[43] Our observations are in general agreement with those of *Grimm* [2013], but in contrast to that author's viewpoint, we argue that the small gravity anomalies and/or positive topography are not necessarily in contradiction with the hypothesis that about 10 km of KREEP-rich materials is present within, or just below, the crust of the Procellarum KREEP Terrane. Though minor differences are found with his model regarding the amplitude of the gravity and topography anomalies, these are largely because his study did not consider the degree-1 gravity signature of the planet (his calculations were done in a Cartesian geometry), and also because his study did not consider gravity signals resulting from the compositional depletion of the mantle.

3.4. Dynamo Generation

[44] Figure 9 (top panel) shows the average heat flow out of the core as a function of time. Similar to symmetric thermal evolution models of the Moon [*Konrad and Spohn*, 1997; *Stegman et al.*, 2003], the core heat flux drops quickly below the adiabat threshold (within about 200 million years), below which a purely thermal dynamo is no longer possible. The adiabatic heat flow depends on the core properties and the largest uncertainty comes from thermal conductivity. We use the same range of plausible core adiabatic heat flux as *Stegman et al.* [2003], which are between 5 and 9 mW/m^2. The effect of the PKT on the core heat flow is small. The small peak at about 4 Ga is due to the onset of mantle convection and the observed difference between nearside and farside is due to the thermal perturbation from the PKT reaching the core. The exact timing of the peak near 4 Ga is dependent on several parameters that control the onset of convection, such as viscosity, and the initial conditions of the thermal model. Nevertheless, even though the effect of the PKT on the average heat flow is small, its spatial distribution on the core-mantle boundary is asymmetrical, as shown in Figure 9. Directly below the PKT, the core is heated while much more heat is extracted from the surroundings.

[45] A long-wavelength pattern could perhaps change the core flow patterns and influence the strength and geometry of a dynamo-generated magnetic field. *Takahashi and Tsunakawa* [2009] have shown that a degree-1 asymmetrical heat flow pattern could lead to a dipolar magnetic field with the dipole axis circulating about a great circle about every 100 years. This magnetic pole variability would certainly

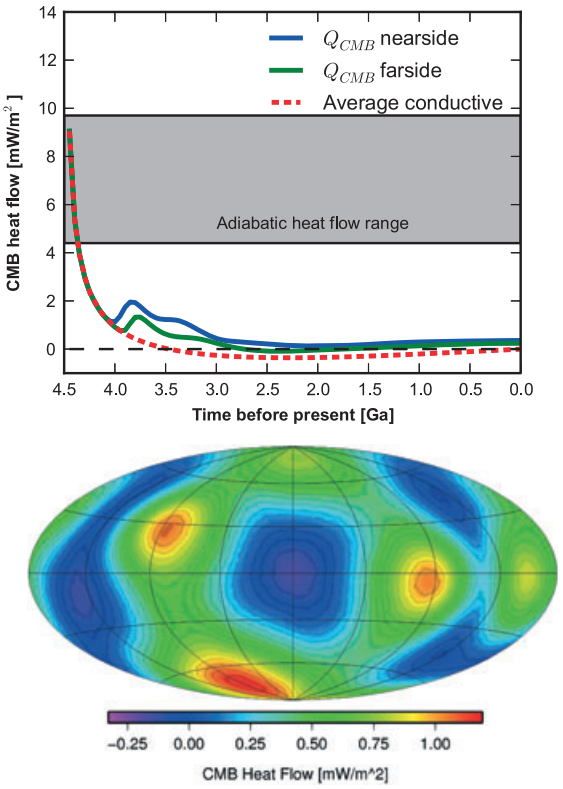

Figure 9. (top) Averaged CMB heat flow for the nearside and farside hemispheres as a function of time, compared with the average for a purely conductive case. (bottom) Present-day core-mantle boundary heat flow centered on the PKT. These results are for our preferred case (model T-0LB).

influence rock magnetization. Crustal rocks would not be magnetized by a directionally stable field, complicating paleomagnetic analyses and interpretations of crustal magnetic anomalies.

[46] We next predict the surface magnetic field at the surface using our core-mantle boundary heat flux and the scaling law for magnetic field strength from *Christensen et al.* [2009]

$$B = f\sqrt{0.63}\sqrt{2\mu_0}\rho^{1/6}(Fq_0)^{1/3}\left(\frac{R_c}{R_p}\right)^3. \quad (14)$$

In this equation, B is the average magnetic field strength on the surface of the Moon, μ_0 is the permeability of free space, ρ is the average core density, F is an efficiency factor, q_0 is the superadiabatic energy flux out of the core, R_c and R_p are the core and lunar radius, respectively, and f is a prefactor expressing the efficiency of ohmic dissipation and the fraction of the field that is in the dipole term exterior to the core. Following *Le Bars et al.* [2011], we use ρ = 7500 kg m^{-3} and f = 0.13. F is calculated from *Christensen et al.* [2009] and is 0.03 when the heat flux does not depend on radius within the core and when there is no inner core present. We note that this parameter is only weakly dependent upon these assumptions. Depending on the assumed initial temperature difference between the mantle and core, the thermal dynamo can last up to about 100 million years and produce a surface magnetic field of about 0.5 μT. Given that F and f are both uncertain, the actual field could perhaps be up to about 10 times larger. Paleomagnetic studies of the oldest lunar samples imply surface fields that are at least 1 μT 4.2 Ga ago [*Garrick-Bethell et al.*, 2009], and perhaps higher than 12 μT between 3.7 and 3.5 Ga [*Shea et al.*, 2012; *Suavet et al.*, 2013]. Even though this thermal dynamo is short-lived and cannot explain all of the paleomagnetic data, it could perhaps explain the magnetization of crustal materials early in lunar history, such as those associated with the South Pole-Aitken impact basin [*Wieczorek et al.*, 2012]. Other models that might explain the younger magnetic signatures include mechanical stirring at the core-mantle boundary from either precession [*Dwyer et al.*, 2011] or changes in the lunar rotation rate from large impact events [*Le Bars et al.*, 2011].

[47] Even if the temporal evolution of the core heat flux is similar among our various simulations and cannot explain a long-lasting lunar dynamo, chemical buoyancy induced by inner core growth might help power the lunar dynamo for a much longer period of time. A recent seismic study suggests that the Moon might possess a solid inner core [*Weber et al.*, 2011], but this remains subject to debate [*Garcia et al.*, 2011]. The liquidus of iron alloys at lunar core pressures is highly dependent on the light element content and can vary between 2050 K for pure iron to 1300 K at the Fe-FeS eutectic. Given that our present-day core-mantle boundary temperature is about 1700 K, it is therefore possible that a portion of the core could have crystallized. Using the phase diagrams from *Buono and Walker* [2011], we find that solid inner core crystallization would have occurred if the sulfur content was less than about 6 wt %. To account for a 240 km inner core as predicted by *Weber et al.* [2011], our core temperatures imply a sulfur content of about 3 wt %.

4. Discussion

[48] As demonstrated in the previous section, mantle convection has a non-negligible influence on the thermal history of the Moon. From Figure 5, we see that the lower mantle is cooler today than it would be for a purely conductive case, and this implies a larger heat flow out of the core between 4 and 3.5 billion years ago (as can also be seen in Figure 9). Similarly, Figure 7 shows that the onset of convection leads to a peak in the production of magma at some time near 4 Ga that the conductive models do not have, due to the upwelling of hot material from depth. Convective models therefore produce more volcanism, even though present-day temperatures are slightly lower than the conductive cases. However, the effects of convection on the gravity observations of Figure 8 are small as the largest temperature differences occur in the lower mantle, which have only a small effect on the surface gravity.

[49] In addition, viscosity has an important effect on mantle dynamics. A lower reference viscosity, appropriate for more wet rheologies, would lead to a more vigorous convection, with a faster onset of convection and more upwelling and downwelling. But as initiation of convection is also dependent on the initial temperature profile, by varying the initial conditions, it is always possible to find scenarios where the initial peak of melting occurs between about 4 and 3 Ga ago. A lower reference viscosity would lead to somewhat lower gravity anomalies as the mantle would be more homogeneous at the present time.

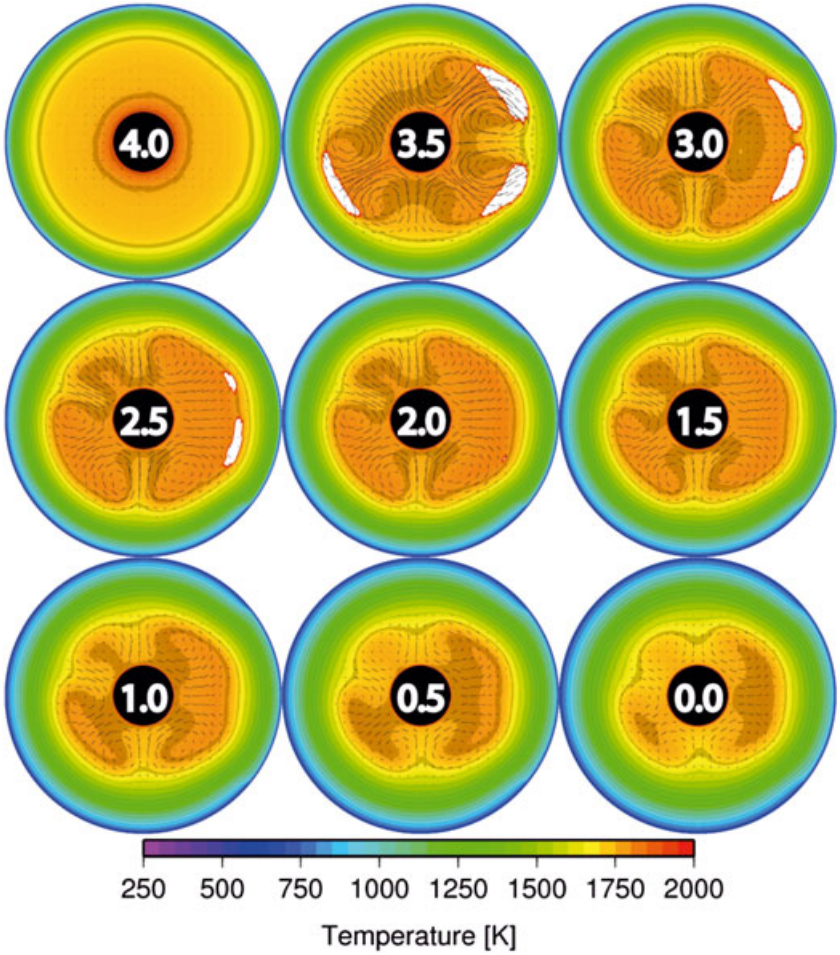

Figure 10. Temperature cross sections of the lunar mantle for a complete thermal evolution for the case with an intermediate initial temperature profile and the KREEP layer redistributed within crust (model "T-0LW"). Numbers correspond to time before present in Ga. The black circle is the lunar core and white corresponds to regions that are partially molten. The streamlines are shown as dashed lines.

[50] Although many of the general features of our thermal model in section 3 are robust to changes in the model parameters (such as the timing and duration of mare volcanism, the spatial distribution of mare volcanism, and dynamo generation), we note that the total volume of generated magma is highly sensitive to the assumed mantle solidus. First, the depletion of the mantle by melting would make it more refractory, causing its solidus temperature to increase. This effect was not considered in our model, nor is it in other lunar evolution models [e.g., *Zhong et al.*, 2000; *Hess and Parmentier*, 2001; *Spohn et al.*, 2001; *Stegman et al.*, 2003; *Ziethe et al.*, 2009], as the composition of the lunar mantle is not well known. Lacking better constraints, the entire mantle was set to a uniform peridotitic composition. Nevertheless, we acknowledge that magma ocean crystallization could have led to a mantle that was zoned in composition. The first magma ocean cumulates would be rich in magnesium, but as crystallization progressed, the cumulates would become increasingly iron rich. To complicate matters, such a sequential cumulate pile is expected to be gravitationally unstable, and a mantle overturn could have brought buoyant nearly pure magnesian-rich dunite to the upper mantle [*Hess and Parmentier*, 1995; *Elkins-Tanton et al.*, 2011]. If this were to occur, the solidus of the upper mantle would likely be higher than that used in our study, and this could dramatically decrease the amount of magma generated by our model.

[51] Heat source partitioning upon melting was also not considered and would help reduce the total amount of melt as a large part of the heat sources would be extracted from the mantle after reaching small melt fractions. This aspect of the melting process has been recognized to be important [*Shearer et al.*, 2006], but was neglected in this study for the sake of simplicity. *Kirk and Stevenson* [1989] found that partitioning of heat sources in the melt reduces the total amount of melt produced in a given model. In addition, a stable mantle stratification, resulting from the gravitational overturn of the crystallized magma ocean cumulates would dramatically decrease convective motions within the mantle. If the density gradient with depth is great enough, the subsequent thermal evolution would be almost entirely due to the process of heat conduction and thus no decompressional melting would occur.

[52] Our models are in general able to match qualitatively the duration of lunar volcanism, the asymmetry in nearside and farside magma production, the location of the youngest

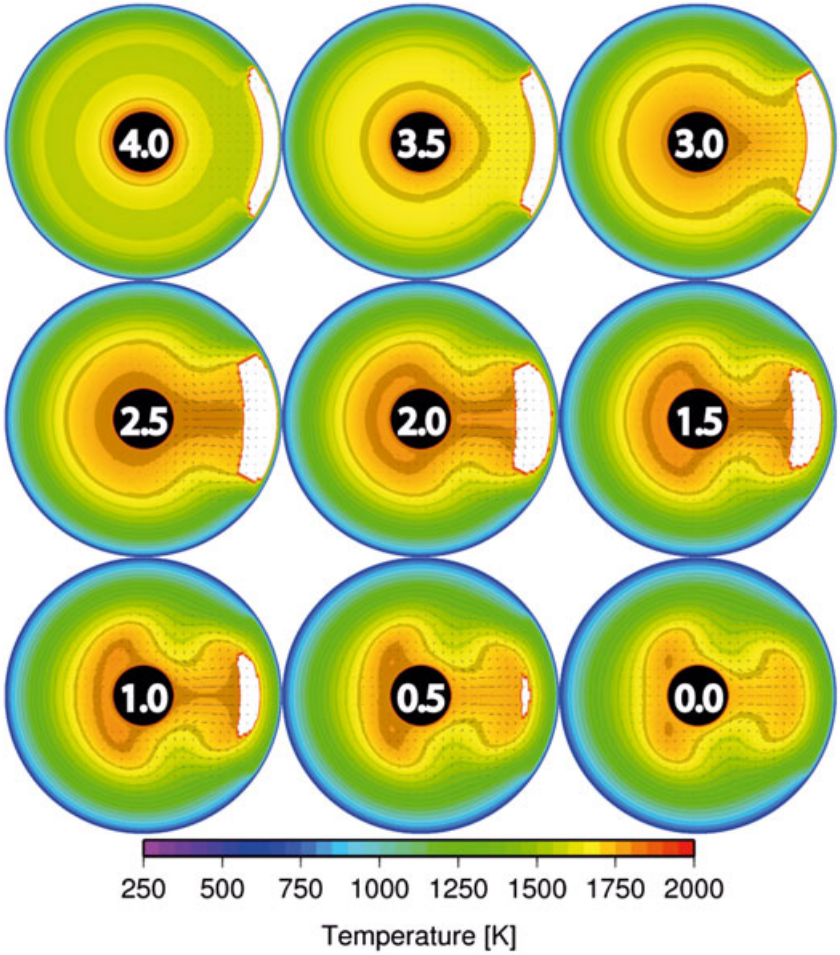

Figure 11. Temperature cross sections of the lunar mantle for a complete thermal evolution for the case with a cold initial temperature profile and the KREEP layer located below the crust (model "A-0LB"). Numbers correspond to time before present in Ga. The black circle is the lunar core and white corresponds to regions that are partially molten. The streamlines are shown as dashed lines.

eruptions, and the present day heat flow measured at the Apollo 15 and 17 landing sites. Nevertheless, we acknowledge that there are two model predictions that are difficult to reconcile. First, our favored models generate about 10 times more magma than is predicted to exist. Second, our models predict several kilometers of dynamic topography within the PKT that is not observed. Regardless, these shortcomings are probably not critical, as there were several model parameters that could not be explored in this study. For example, changing the thickness of the KREEP layer or its distribution within the crust and mantle would help obtaining a better fit of these constraints. In addition, the mantle solidus could be modified to account for a post mantle overturn scenario. Finally, crustal thickness variations, which might be expected to occur during the formation of the PKT were not considered and would directly influence the predicted surface uplift.

5. Conclusions

[53] A 3D thermochemical convection code was used to study the influence of an enrichment in heat sources in the Procellarum KREEP Terrane on the nearside of the Moon. Our simulations show that the enhancement in heat production in this region partially melts the underlying mantle to depths of about 600 km over a duration of about 3 to 3.5 billion years. In contrast, the lower heat production on the farside, combined with the initiation of mantle convection, gives rise to farside magma production rates that are 10 times smaller than the nearside, and which lasts for only about 0.5 billion years. These results are consistent with the observed distribution of the mare basalts, and well as the duration of mare volcanism as inferred from lunar samples and crater counting techniques.

[54] Our results imply that a large temperature anomaly is preserved at the present day below the PKT. This result has immediate implications for the interpretation of electromagnetic sounding data [*Grimm*, 2013], the modeling of tidal deformation Love numbers [*Zhong et al.*, 2012], the concentration of tidal stresses, as well as the interpretation of the Apollo seismic data. This thermal anomaly predicts uplift of the surface in the PKT, and when combined with the compositional depletion of the mantle and mare basalts, a small gravity anomaly as well. If the lithosphere were weak, the different gravity contributions would compensate to an almost zero gravity anomaly with a surface uplift of

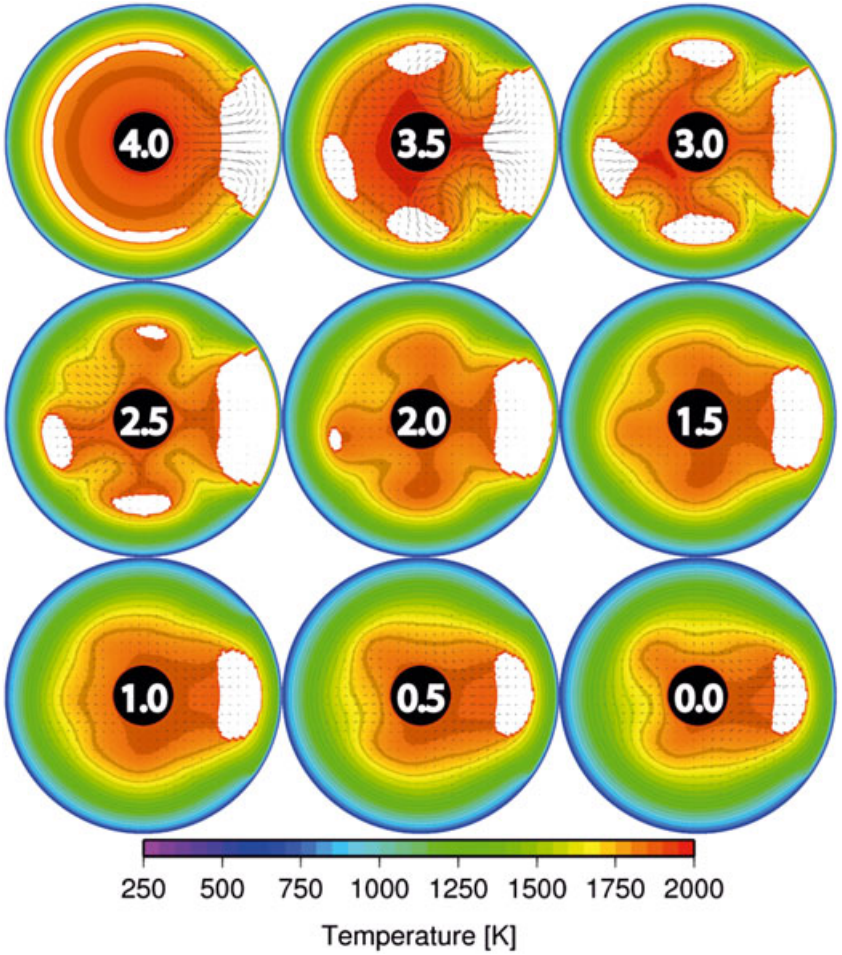

Figure 12. Temperature cross sections of the lunar mantle for a complete thermal evolution for the case with a hot initial temperature profile and the KREEP layer located below the crust (model "D-0LB"). Numbers correspond to time before present in Ga. The black circle is the lunar core and white corresponds to regions that are partially molten. The streamlines are shown as dashed lines.

a few kilometers. For a rigid lithosphere, no uplift is generated, but the negative gravity anomaly would be larger. For the strengthless lithosphere interpretation, this discrepancy could be resolved if the crust in the PKT were 10–20 km thinner than the surroundings, or if the nearside mantle were denser than average. Both possibilities are plausible given the unique manner by which this province formed.

[55] Finally, using the predicted core temperatures and core heat flux from our model, we show that the Moon could have powered a dynamo with a surface field strength of

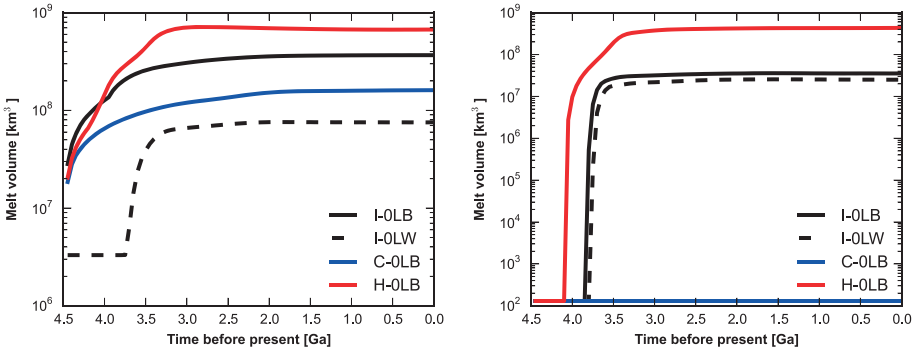

Figure 13. Cumulate melt volume on the (left) nearside and (right) farside. The color indicates the initial temperature profile (black is intermediate, blue is cold and red is hot). Solid lines correspond to cases with the KREEP layer located below the crust whereas the dashed line corresponds to KREEP initially redistributed within the crust. The nomenclature follows Table 3.

about 1 μT for only the first 200 million years of its evolution. This could perhaps explain some of the oldest crustal magnetic anomalies, but not the paleomagnetic results that require the dynamo to have lasted until about 3.56 billion years ago [*Suavet et al.*, 2013]. Nevertheless, if the sulfur content of the lunar core is less than 6 wt %, our thermal history implies that some portion of the core would have crystallized to form a solid inner core. Not only is this consistent with recent seismic data, but it also offers the possibility of driving a dynamo based on core crystallization for a much longer period of time.

[56] **Acknowledgments.** This work was performed using the High Performance Computing resources from GENCI-CCRT and from JUROPA/HPC-FF. M. Laneuville wishes to thank A.-C. Plesa for her continuous help using Gaia. N. Tosi acknowledges support from the Deutsche Forschungs Gemeinschaft (grant 704/1-1). This work was partially funded by the UnivEarths LabEx program of Sorbonne Paris Cité (ANR-10-LABX-0023 and ANR-11-IDEX-0005-02) as well as by the Helmholtz Association through the research alliance "Planetary Evolution and Life." The authors also wish to thank F. Nimmo, S. Zhong, and an anonymous reviewer for detailed comments that helped improve this manuscript.

References

Andrews-Hanna, J. C., et al. (2013), Ancient igneous intrusions and early expansion of the Moon revealed by GRAIL gravity gradiometry, *Science*, *339*, 675–678, doi:10.1126/science.1231753.

Antonenko, I., J. W. Head, J. Mustard, and B. R. Hawke (1995), Criteria for the detection of lunar cryptomaria, *Earth Moon Planets*, *69*, 141–172, doi:10.1007/BF00613096.

Beuthe, M. (2008), Thin elastic shells with variable thickness for lithospheric flexure of one-plate planets, *Geophys. J. Int.*, *172*, 817–841, doi:10.1111/j.1365-246X.2007.03671.x.

Buono, A. S., and D. Walker (2011), The Fe-rich liquidus in the Fe–FeS system from 1 bar to 10 GPa, *Geochim. Cosmochim. Acta*, *75*, 2072–2087, doi:10.1016/j.gca.2011.01.030.

Byrne, C. J. (2007), A large basin on the nearside of the Moon, *Earth Moon Planets*, *101*, 153–188, doi:10.1007/s11038-007-9225-8.

Christensen, U. R. (1984), Convection with pressure- and temperature-dependent non-Newtonian rheology, *Geophys. J. R. Astron. Soc.*, *77*, 343–384, doi:10.1111/j.1365-246X.1984.tb01939.x.

Christensen, U. R., V. Holzwarth, and A. Reiners (2009), Energy flux determines magnetic field strength of planets and stars, *Nature*, *457*, 167–169, doi:10.1038/nature07626.

Crosby, A., and D. McKenzie (2005), Measurements of the elastic thickness under ancient lunar terrain, *Icarus*, *173*, 100–107, doi:10.1016/j.icarus.2004.07.017.

de Smet, J. H., A. P. van den Berg, and N. J. Vlaar (1999), The evolution of continental roots in numerical thermo-chemical mantle convection models including differentiation by partial melting, *Lithos*, *48*, 153–170, doi:10.1016/S0024-4937(99)00028-6.

Dwyer, C. A., D. J. Stevenson, and F. Nimmo (2011), A long-lived lunar dynamo driven by continuous mechanical stirring, *Nature*, *479*, 212–214, doi:10.1038/nature10564.

Elkins-Tanton, L. T., J. A. Van Orman, B. H. Hager, and T. L. Grove (2002), Re-examination of the lunar magma ocean cumulate overturn hypothesis: Melting or mixing is required, *Earth Planet. Sci. Lett.*, *196*, 239–249, doi:10.1016/S0012-821X(01)00613-6.

Elkins-Tanton, L. T., S. Burgess, and Q.-Z. Yin (2011), The lunar magma ocean: Reconciling the solidification process with lunar petrology and geochronology, *Earth Planet. Sci. Lett.*, *304*, 326–336, doi:10.1016/j.epsl.2011.02.004.

Garcia, R., J. Gagnepain-Beyneix, S. Chevrot, and P. Lognonné (2011), Very preliminary reference Moon model, *Phys. Earth Planet. Inter.*, *188*, 96–113, doi:10.1016/j.pepi.2011.06.015.

Garrick-Bethell, I., B. P. Weiss, D. L. Shuster, and J. Buz (2009), Early lunar magnetism, *Science*, *323*, 356–359, doi:10.1126/science.1166804.

Ghods, A., and J. Arkani-Hamed (2007), Impact-induced convection as the main mechanism for formation of lunar mare basalts, *J. Geophys. Res.*, *112*, E03005, doi:10.1029/2006JE002709.

Golle, O., C. Dumoulin, G. Choblet, and O. Čadek (2012), Topography and geoid induced by a convecting mantle beneath an elastic lithosphere, *Geophys. J. Int.*, *189*, 55–72, doi:10.1111/j.1365-246X.2012.05364.x.

Grimm, R. E. (2013), Geophysical constraints on the lunar Procellarum KREEP Terrane, *J. Geophys. Res. Planets*, *118*, 768–778, doi:10.1029/2012JE004114.

Haruyama, J., et al. (2009), Long-lived volcanism on the lunar farside revealed by SELENE Terrain Camera, *Science*, *323*, 905–908, doi:10.1126/science.1163382.

Haskin, L. A. (1998), The Imbrium impact event and the thorium distribution at the lunar highlands surface, *J. Geophys. Res.*, *103*, 1679–1689, doi:10.1029/97JE03035.

Hess, P. C., and E. M. Parmentier (1995), A model for the thermal and chemical evolution of the Moon's interior: Implications for the onset of mare volcanism, *Earth Planet. Sci. Lett.*, *134*, 501–514, doi:10.1016/0012-821X(95)00138-3.

Hess, P. C., and E. M. Parmentier (2001), Thermal evolution of a thicker KREEP liquid layer, *J. Geophys. Res.*, *106*, 28,023–28,032, doi:10.1029/2000JE001416.

Hiesinger, H., J. W. Head, U. Wolf, R. Jaumann, and G. Neukum (2003), Ages and stratigraphy of mare basalts in Oceanus Procellarum, mare Nubium, mare Cognitum, and mare Insularum, *J. Geophys. Res.*, *108*(E7), 5065, doi:10.1029/2002JE001985.

Hirschmann, M. M. (2000), Mantle solidus: Experimental constraints and the effects of peridotite composition, *Geochem. Geophys. Geosyst.*, *1*, 1042, doi:10.1029/2000GC000070.

Hüttig, C., and K. Stemmer (2008), Finite volume discretization for dynamic viscosities on Voronoi grids, *Phys. Earth Planet. Inter.*, *171*, 137–146, doi:10.1016/j.pepi.2008.07.007.

Ita, J., and S. D. King (1994), Sensitivity of convection with an endothermic phase change to the form of governing equations, initial conditions, boundary conditions, and equation of state, *J. Geophys. Res.*, *99*, 15,919–15,938, doi:10.1029/94JB00852.

Jolliff, B. L., J. J. Gillis, L. A. Haskin, R. L. Korotev, and M. A. Wieczorek (2000), Major lunar crustal terranes: Surface expressions and crust-mantle origins, *J. Geophys. Res.*, *105*, 4197–4216, doi:10.1029/1999JE001103.

Jutzi, M., and E. Asphaug (2011), Forming the lunar farside highlands by accretion of a companion moon, *Nature*, *476*, 69–72, doi:10.1038/nature10289.

Kamata, S., et al. (2013), Viscoelastic deformation of lunar impact basins: Implications for heterogeneity in the deep crustal paleo-thermal state and radioactive element concentration, *J. Geophys. Res. Planets*, *118*, 398–415, doi:10.1002/jgre.20056.

Karato, S., and P. Wu (1993), Rheology of the upper mantle: A synthesis, *Science*, *260*, 771–778, doi:10.1126/science.260.5109.771.

Khan, A., and K. Mosegaard (2002), An inquiry into the lunar interior: A nonlinear inversion of the Apollo lunar seismic data, *J. Geophys. Res.*, *107*, 5036, doi:10.1029/2001JE001658.

Kirk, R. L., and D. J. Stevenson (1989), The competition between thermal contraction and differentiation in the stress history of the Moon, *J. Geophys. Res.*, *94*, 12,133–12,144, doi:10.1029/JB094iB09p12133.

Konrad, W., and T. Spohn (1997), Thermal history of the Moon—Implications for an early core dynamo and post-accretional magmatism, *Adv. Space Res.*, *19*, 1511–1521, doi:10.1016/S0273-1177(97)00364-5.

Korotev, R. L. (2000), The great lunar hot spot and the composition and origin of the Apollo mafic (LKFM) impact-melt breccias, *J. Geophys. Res.*, *105*, 4317–4346, doi:10.1029/1999JE001063.

Langseth, M. G., S. J. Keihm, and K. Peters (1976), Revised lunar heat-flow values, *Proc. Lunar Sci. Conf.*, *7*, 3143–3171.

Lawrence, D. J., W. C. Feldman, B. L. Barraclough, A. B. Binder, R. C. Elphic, S. Maurice, and D. R. Thomsen (1998), Global elemental maps of the Moon: The *Lunar Prospector* gamma-ray spectrometer, *Science*, *281*, 1484–1489, doi:10.1126/science.281.5382.1484.

Lawrence, D. J., R. C. Elphic, W. C. Feldman, T. H. Prettyman, O. Gasnault, and S. Maurice (2003), Small-area thorium features on the lunar surface, *J. Geophys. Res.*, *108*, 5102, doi:10.1029/2003JE002050.

Le Bars, M., M. A. Wieczorek, Ö. Karatekin, D. Cébron, and M. Laneuville (2011), An impact-driven dynamo for the early Moon, *Nature*, *479*, 215–218, doi:10.1038/nature10565.

Lognonné, P., J. Gagnepain-Beyneix, and H. Chenet (2003), A new seismic model of the Moon: Implications for structure, thermal evolution and formation of the Moon, *Earth Planet. Sci. Lett.*, *211*, 27–44, doi:10.1016/S0012-821X(03)00172-9.

Loper, D. E., and C. L. Werner (2002), On lunar asymmetries 1. Tilted convection and crustal asymmetry, *J. Geophys. Res.*, *107*, 5046, doi:10.1029/2000JE001441.

Metzger, A. E., E. L. Haines, R. E. Parker, and R. G. Radocinski (1977), Thorium concentrations in the lunar surface. I—Regional values and crustal content, in *Proc. Lunar Planet. Sci. Conf.,* vol. 8, pp. 949–999, LPI, Houston, Tex.

Mimoun, D., et al. (2012), Farside explorer: Unique science from a mission to the farside of the Moon, *Exp. Astron.*, *33*, 529–585, doi:10.1007/s10686-011-9252-3.

Morota, T., et al. (2009), Mare volcanism in the lunar farside Moscoviense region: Implication for lateral variation in magma production of the Moon, *Geophys. Res. Lett.*, *36*, L21202, doi:10.1029/2009GL040472.

Neumann, G. A., M. T. Zuber, D. E. Smith, and F. G. Lemoine (1996), The lunar crust: Global structure and signature of major basins, *J. Geophys. Res.*, *101*, 16,841–16,864, doi:10.1029/96JE01246.

Parmentier, E. M., S. Zhong, and M. T. Zuber (2002), Gravitational differentiation due to initial chemical stratification: Origin of lunar asymmetry by the creep of dense KREEP?, *Earth Planet. Sci. Lett.*, *201*, 473–480, doi:10.1016/S0012-821X(02)00726-4.

Plesa, A.-C., N. Tosi, and C. Hüttig (2013), Thermo-chemical convection in planetary mantles, in *Integrated Information and Computing Systems for Natural, Spatial, and Social Sciences*, edited by C.-P. Rückemann, IGI Global, Hershey, Pa, doi:10.4018/978-1-4666-2190-9.ch015.

Qin, C., A. C. Muirhead, and S. Zhong (2012), Correlation of deep moonquakes and mare basalts: Implications for lunar mantle structure and evolution, *Icarus*, *220*, 100–105, doi:10.1016/j.icarus.2012.04.023.

Richards, M. A., and B. H. Hager (1984), Geoid anomalies in a dynamic Earth, *J. Geophys. Res.*, *89*, 5987–6002, doi:10.1029/JB089iB07p05987.

Roberts, J., and S. Zhong (2006), Degree-1 convection in the Martian mantle and the origin of the hemispheric dichotomy, *J. Geophys. Res.*, *111*, E06013, doi:10.1029/2005JE002668.

Schubert, G., D. L. Turcotte, and E. R. Oxburgh (1969), Stability of planetary interiors, *Geophys. J. R. Astron. Soc.*, *18*, 441–460.

Scott, D. R., and D. J. Stevenson (1989), A self-consistent model of melting, magma migration and buoyancy-driven circulation beneath mid-ocean ridges, *J. Geophys. Res.*, *94*, 2973–2988.

Shea, E. K., B. P. Weiss, W. S. Cassata, D. L. Shuster, S. M. Tikoo, J. Gattacceca, T. L. Grove, and M. D. Fuller (2012), A long-lived lunar core dynamo, *Science*, *335*, 453–456, doi:10.1126/science.1215359.

Shearer, C., et al. (2006), Thermal and magmatic evolution of the Moon, *Rev. Mineral. Geochem.*, *60*, 365–518.

Spohn, T., W. Konrad, D. Breuer, and R. Ziethe (2001), The longevity of lunar volcanism: Implications of thermal evolution calculations with 2D and 3D mantle convection models, *Icarus*, *149*, 54–65, doi:10.1006/icar.2000.6514.

Stegman, D. R., A. M. Jellinek, S. A. Zatman, J. R. Baumgardner, and M. A. Richards (2003), An early lunar core dynamo driven by thermochemical mantle convection, *Nature*, *421*, 143–146, doi:10.1038/nature01267.

Suavet, C., B. P. Weiss, W. S. Cassata, D. L. Shuster, J. Gattacceca, L. Chan, I. Garrick-Bethell, J. W. Head, T. L. Grove, and M. D. Fuller (2013), Persistence and origin of the lunar core dynamo, *Proc. Natl. Acad. Sci. U.S.A.*, *18*, 1–6, doi:10.1073/pnas.1300341110.

Takahashi, F., and H. Tsunakawa (2009), Thermal core-mantle coupling in an early lunar dynamo: Implications for a global magnetic field and magnetosphere of the early Moon, *Geophys. Res. Lett.*, *36*, L24202, doi:10.1029/2009GL041221.

Taylor, S. R. (1982), *Planetary Science: A Lunar Perspective*, 481 pp., Lunar and Planetary Institute, Houston.

Taylor, S. R., G. J. Taylor, and L. A. Taylor (2006), The Moon: A Taylor perspective, *Geochim. Cosmochim. Acta*, *70*, 5904–5918, doi:10.1016/j.gca.2006.06.262.

Turcotte, D. L., R. J. Willemann, W. F. Haxby, and J. Norberry (1981), Role of membrane stresses in the support of planetary topography, *J. Geophys. Res.*, *86*(B5), 3951–3959.

van der Meer, D. G., W. Spakman, D. J. J. van Hinsbergen, M. L. Amaru, and T. H. Torsvik (2009), Towards absolute plate motions constrained by lower-mantle slab remnants, *Nat. Geosci.*, *3*, 36–40, doi:10.1038/ngeo708.

van Keken, P. E., S. D. King, H. Schmeling, U. R. Christensen, and D. N. M. Doin (1997), A comparison of methods for the modeling of thermochemical convection, *J. Geophys. Res.*, *102*, 22,477–22,495, doi:10.1029/97JB01353.

Warren, P. H. (2001), Compositional structure within the lunar crust as constrained by *Lunar Prospector* thorium data, *Geophys. Res. Lett.*, *28*, 2565–2568, doi:10.1029/2000GL012739.

Warren, P. H., and K. L. Rasmussen (1987), Megaregolith insulation, internal temperatures, and bulk uranium content of the Moon, *J. Geophys. Res.*, *92*, 3453–3465, doi:10.1029/JB092iB05p03453.

Warren, P. H., and J. T. Wasson (1979), The origin of KREEP, *Rev. Geophys. Space Phys.*, *17*, 73–88, doi:10.1029/RG017i001p00073.

Warren, P. H., and J. T. Wasson (1980), Further foraging for pristine nonmare rocks: Correlations between geochemistry and longitude, in *Proc. Lunar Planet. Sci. Conf.,* vol. 11, pp. 431–470, LPI, Houston, Tex.

Wasson, J. T., and P. H. Warren (1980), Contribution of the mantle to the lunar asymmetry, *Icarus*, *44*, 752–771, doi:10.1016/0019-1035(80)90142-6.

Watters, T. R., et al. (2010), Evidence of recent thrust faulting on the Moon revealed by the Lunar Reconnaissance Orbiter Camera, *Science*, *329*(5994), 936–940, doi:10.1126/science.1189590.

Watts, A. B., and S. Zhong (2000), Observations of flexure and the rheology of oceanic lithosphere, *Geophys. J. Int.*, *142*, 855–875.

Weber, R. C., P. Y. Lin, E. J. Garnero, Q. Williams, and P. Lognonne (2011), Seismic detection of the lunar core, *Science*, *331*, 309–312, doi:10.1126/science.1199375.

White, S. M., J. A. Crisp, and F. J. Spera (2006), Long-term volumetric eruption rates and magma budgets, *Geochem. Geophys. Geosyst.*, *7*, Q03010, doi:10.1029/2005GC001002.

Wieczorek, M., et al. (2006), The constitution and structure of the lunar interior, *Rev. Mineral. Geochem.*, *60*, 221–364.

Wieczorek, M. A. (2007), Gravity and topography of the terrestrial planets, in *Treatise on Geophysics, 10*, edited by T. Spohn, pp. 165–206, Elsevier, Amsterdam.

Wieczorek, M. A., and R. J. Phillips (2000), The "Procellarum KREEP Terrane": Implications for mare volcanism and lunar evolution, *J. Geophys. Res.*, *105*, 20,417–20,430, doi:10.1029/1999JE001092.

Wieczorek, M. A., M. T. Zuber, and R. J. Phillips (2001), The role of magma buoyancy on the eruption of lunar basalts, *Earth Planet. Sci. Lett.*, *185*, 71–83, doi:10.1016/S0012-821X(00)00355-1.

Wieczorek, M. A., B. P. Weiss, and S. T. Stewart (2012), An impactor origin for lunar magnetic anomalies, *Science*, *335*, 1212–1215, doi:10.1126/science.1214773.

Wieczorek, M. A., et al. (2013), The crust of the Moon as seen by GRAIL, *Science*, *339*, 671–675, doi:10.1126/science.1231530.

Williams, K. K., and M. T. Zuber (1998), Measurement and analysis of lunar basin depths from Clementine Altimetry, *Icarus*, *122*, 107–122.

Zhong, S. (2002), Effects of lithosphere on the long-wavelength gravity anomalies and their implications for the formation of the Tharsis rise on Mars, *J. Geophys. Res.*, *107*, 5054, doi:10.1029/2001JE001589.

Zhong, S., E. M. Parmentier, and M. T. Zuber (2000), A dynamic origin for the global asymmetry of lunar mare basalts, *Earth Planet. Sci. Lett.*, *177*, 131–140, doi:10.1016/S0012-821X(00)00041-8.

Zhong, S., C. Qin, A. Geruo, and J. Wahr (2012), Can tidal tomography be used to unravel the long-wavelength structure of the lunar interior?, *Geophys. Res. Lett.*, *39*, L15201, doi:10.1029/2012GL052362.

Ziethe, R., K. Seiferlin, and H. Hiesinger (2009), Duration and extent of lunar volcanism: Comparison of 3D convection models to mare basalt ages, *Planet. Space Sci.*, *57*, 784–796, doi:10.1016/j.pss.2009.02.002.

Zuber, M. T., et al. (2013), Gravity field of the Moon from the Gravity Recovery and Interior Laboratory (GRAIL) Mission, *Science*, *339*, 668–671, doi:10.1126/science.1231507.